Table 2 Peptide sequence on a fibronectine outer loop library constructed in the present study

No.	Sequence	No.	Sequence	No.	Sequence
67	S D I T A	90	S R N S I	113	A V T V R
68	D I T A N	91	R N S I T	114	V T V R Y
69	I T A N S	92	N S I T T	115	T V R Y Y
70	I A P R T	93	S I T T L	116	G E T G G
71	A P R T I	94	I T T L T	117	E T G G N
72	P R T I T	95	T T L T N	118	T G G N S
73	R T I T G	96	T L T N L	119	G G N S P
74	H P E H F	97	L T N L T	120	G N S P V
75	P E H F S	98	T N L T P	121	N S P V Q
76	E H F S G	99	N L T P G	122	V P G S K
77	H F S G R	100	L T P G T	123	P G S K S
78	F S G R P	101	V A L N G	124	G S K S T
79	S G R P R	102	A L N G R	125	S G L K P
80	G R P R E	103	L N G R E	126	G L K P G
81	R P R E D	104	N G R E E	127	L K P G V
82	P R E D R	105	E V V A A	128	K P G V D
83	R E D R V	106	V V A A T	129	G R G D S
84	E D R V P	107	V A A T P	130	R G D S P
85	D R V P H	108	A A T P T		AAAAA
86	R V P H S	109	A T P T S		RGDS
87	V P H S R	110	D A P A V		no peptide
88	P H S R N	111	A P A V T		
89	H S R N S	112	P A V T V		

2. Results and Discussion

In **Table 2**, the peptide sequences, assayed in the present paper are listed. The sequence of fibronectin was divided into 2 parts. The latter part was selected for screening because RGDS peptide was included and 63 pentamer peptides in the latter part were tested.

Assay results are shown in **Figure 1**. High adhesion ratios were confirmed with sequence nos. 129 and 130, which are GRGDS and RGDSP, respectively, and those are containing adhesion motif of RGDS. There are many peptides with a high adhesion ratio in mGEC (Figure 1(b)) compared with that of mLEC (Figure 1(a)). Sequence nos. 124 (GSKST) and 126 (GLKPG) showed a high adhesion ratio in both ECs, and those were found to be also high for HUVEC (Figure 1(c)). From nos. 67 to 128, except for two sequences containing of RGDS, only 8 peptides showed a higher adhesion ratio for mGEC compared with that for HUVEC, which were dissectionally existed in the whole region. There was only one such peptide for mLEC, which was no. 126. From these findings, it was found that two ECs are possible to be discriminated by pentamer peptides, even though two cells are categorized into a type of epithelial cell. This suggests that such peptides behave as a tissue specific molecular tag.

As a further experiment, adhesion peptides for mesenchymal stem cell (MSC), which is a multipotent cell resident in bone marrow, was also demonstrated and compared with those for two ECs. Results are shown in Figure 1(d). Sequence no. 126 shows the highest adhesion ratio for MSC. From the adhesion ratio for all 63 peptides, it was found that sequences nos. 95 to 98 show relatively low adhesion ratios and high adhesion ratios were obtained from sequences the nos. 112 to 116. This pattern was similar to that of mLEC. Although a partly similar pattern was obtained for HUVEC (Figure 1(c)), the ratios of sequences nos. 70 to 90 were different from those of MSC and mLEC, and those peptides showed relatively high adhesion ratios for HUVEC. As specific peptides with high adhesion ratios for MSC, 4 peptides such as nos. 99 (NLTPG), 102 (ALNGR), 114 (VTVRY), and 116 (GETGG) were identified.

Peptides with high adhesion ratios for each cell are listed in **Table 3**. Identified peptides for mGEC were specified as T containing peptides. Sequences no. 95 (TTLTN) and no. 98 (TNLTP) are similar to each other. It was found that adhesive peptides for mLEC are similar to those of MSC, rather than HUVEC.

Glomerular epitherial cell (GEC) (known as podocyte) are located on the outer surface of the glomerular capillary wall and act as a filtration barrier. GEC injury causes various kidney diseases. Lung epitherial cells (LEC) are also positioned in lung tissue as the outer cell layer. LEC also forms a continuous barrier against environmental exposure. Lung disease is caused by epithelial cell injury based on viral infection, allergic reaction, or LEC apoptosis on

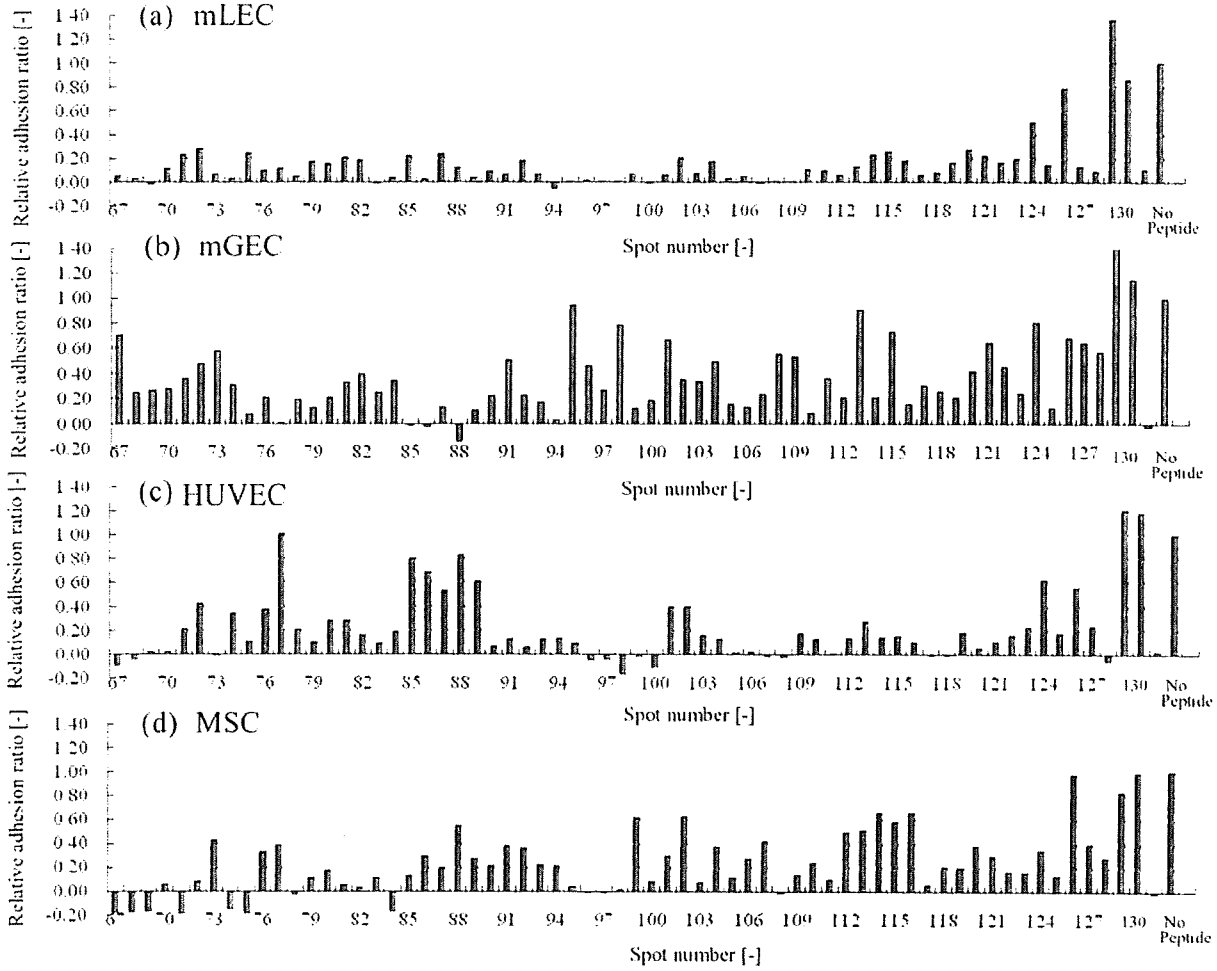

Fig. 1 Relative cell adhesion ratios for mLEC(a), mGEC(b), HUVEC(c) and MSC(d) against partial peptide library from fibronectin outer loop

Table 3 List of high adhesive peptide for each cells

Cell	High adhesive peptides* (Peptide No./Sequence)			
mLEC	126/GLKPG			
mGEC	95/TTLTN	113/AVTVR	124/GSKST	98/TNLTP
HUVEC	77/HFSGR	88/PHSRN	85/DRVPH	
MSC	126/GLKPG			

*Peptide with relative adhesion ratio of more than 75% were listed.

autoimmune reaction. Therefore, the molecules targeting and adhering on GEC or LEC are very attractive substances because such molecules are applicable for drug delivery therapy. Nagao *et al.* (2007) reported that adhesion protein expression such as ICAM-1, VCAM-1 and E-selectin was increased by treatment of anti-recombinant mouse myeloperoxidase (MPO) IgG. MPO-IgG treatment is an animal model for rapidly progressive (crescentic) IgA glomerulonephritis caused by antineutrophil cytoplasmic autoantibody (ANCA) and the up-regulated adhesion proteins mentioned above are very attractive as target proteins for diagnosis or treatment. When targeting molecules such as peptides are intravenously administered, contact with endothelial cells is inevitable. Peptides which show low adhesion ability for endothelial cells should be screened. In the present study, sequence no. 96 (TTLTN) and no. 98 (TNLTP) have great potential as a GEC targeting molecule. For LEC, GLKPG showed the highest adhesion ratio, although the peptide can also adhere to HUVEC.

It should be noted that RGDS motif can adhere to all cells tested here without any specificity. It is likely that the peptides selected in the present paper can function as more selective homing peptides compared with RGDS peptide. The peptides are attractive candidates for tissue specific targeting, although further demonstration of whether or not these peptides have a significant affinity against those epithelial-type cells

compared with other organ cells would be required. Amino acid substitution from candidate sequences has much possibility for the design of improved peptides with high specificity (Kaga *et al.*, 2007). We have also reported the computationally-assisted peptide screening method from random peptide library (Kaga *et al.*, 2008). By using these methods, the development of a superior peptide is anticipated.

Conclusions

Using a peptide array-based cell system, screening of cell adhesive peptides has been investigated against two epithelial-type cells (mLEC and mGEC), and one endothelial cell (HUVEC). From pentamer peptide sequences of human fibronectin type III domain, some cell-specific peptides were found; eight adhesive peptides were found for mGEC as peptides with higher adhesion activity compared with HUVEC. The results suggest that a tissue specific adhesion peptides can be designed, which has the potential for the development of a tissue specific molecular tag.

Acknowledgments

This study was partly performed through Special Coordination Funds for Promoting Science and Technology of the Ministry of Education, Culture, Sports, Science and Technology, of the Japanese Government.

Literature Cited

Frank, R.; "The SPOT-Synthesis Technique. Synthetic Peptide Arrays on Membrane Supports—Principles and Applications," *J. Immunol. Methods*, **267**, 13–26 (2002)

Kaga, C., M. Okochi, M. Nakanishi, H. Hayashi, R. Kato and H. Honda; "Screening of a Novel Octamer Peptide, CNSCWSKD, That Induces Caspase-Dependent Cell Death," *Biochem. Biophys. Res. Commun.*, **362**, 1063–1068 (2007)

Kaga, C., M. Okochi, Y. Tomita, R. Kato and H. Honda; "Computationally-Assisted Screening and Design of Cell-Interactive Peptides by a Cell-Based Assay Using Peptide Arrays and a Fuzzy Neural Network Algorithm," *Biotechniques*, **44**, 393–402 (2008)

Kato, R., C. Kaga, M. Kunimatsu, T. Kobayashi and H. Honda; "Peptide Array-Based Interaction Assay of Solid-Bound Peptides and Anchorage-Dependant Cells and Its Effectiveness in Cell-Adhesive Peptide Design," *J. Biosci. Bioeng.*, **101**, 485–495 (2006)

Kumer, A. and J. Schneider-Mergener; "Synthesis and Screening of Peptide Libraries on Continuous Cellulose Membrane Supports," *Methods. Mol. Biol.*, **87**, 25–39 (1998)

Nagao, T., M. Matsumura, A. Mabuchi, A. Ishida-Okawara, O. Koshio, T. Nakayama, H. Minamitani and K. Suzuki; "Up-Regulation of Adhesion Molecule Expression on Glomerular Endothelial Cells by Anti-Myeloperoxidase Antibody," *Nephrol. Dial. Transplant.*, **22**, 77–87 (2007)

Nomura, S., C. Kaga, R. Kato, M. Okochi and H. Honda; "Screening of Cell Adhesive Peptide from the Human Laminin-5 $\alpha 3$ Chain Globular 2 and 3 Domains," *J. Chem. Eng. Japan*, **41**, 206–209 (2008)

Okochi, M., M. Nakanishi, R. Kato, T. Kobayashi and H. Honda; "High-Throughput Screening of Cell Death Inducible Short Peptides from TNF-Related Apoptosis-Inducing Ligand Sequence," *FEBS Lett.*, **580**, 885–889 (2006)

Okochi, M., S. Nomura, C. Kaga and H. Honda; "Peptide Array-Based Screening of Human Mesenchymal Stem Cell-Adhesive Peptides Derived from Fibronectin type III Domain," *Biochem. Biophys. Res. Commun.*, **371**, 85–89 (2008)

The Journal of Immunology

IL-10 Is a Negative Regulatory Factor of CAWS-Vasculitis in CBA/J Mice as Assessed by Comparison with Bruton's Tyrosine Kinase-Deficient CBA/N Mice

Noriko N. Miura, Motohiko Komai, Yoshiyuki Adachi, Naoki Osada, Yosuke Kameoka, Kazuo Suzuki and Naohito Ohno

J. Immunol. 2009;183;3417-3424; originally published online Aug 12, 2009;
doi:10.4049/jimmunol.0802484
http://www.jimmunol.org/cgi/content/full/183/5/3417

The Journal of Immunology is published twice each month by The American Association of Immunologists, Inc., 9650 Rockville Pike, Bethesda, MD 20814-3994.

Print ISSN: 0022-1767 Online ISSN: 1550-6606.

IL-10 Is a Negative Regulatory Factor of CAWS-Vasculitis in CBA/J Mice as Assessed by Comparison with Bruton's Tyrosine Kinase-Deficient CBA/N Mice[1]

Noriko N. Miura,* Motohiko Komai,* Yoshiyuki Adachi,* Naoki Osada,† Yosuke Kameoka,† Kazuo Suzuki,§‡ and Naohito Ohno[2]*

Candida albicans water-soluble fraction (CAWS), a mannoprotein-β-glucan complex obtained from the culture supernatant of *C. albicans* NBRC1385, exhibits vasculitis-inducing activity (CAWS-vasculitis) in mice. The sensitivity to CAWS-vasculitis varies greatly among mouse strains. This study examined the factors contributing to or inhibiting CAWS-vasculitis using CAWS-vasculitis-resistant CBA/J mice and Bruton's tyrosine kinase-deficient CBA/N mice, which is a CAWS-vasculitis-sensitive strain that has the same origin as CBA/J mice. After stimulation with various kinds of pathogen-associated molecular patterns, the production of inflammatory cytokines IL-6 and IFN-γ was induced in CBA/N mice, whereas that of immunosuppressive IL-10 was induced in CAWS-vasculitis-resistant CBA/J mice. Furthermore, the production of tissue inhibitor of metalloproteinase 1, an endogenous matrix metalloproteinase inhibitor, was observed in CBA/J mice. The results strongly suggest that the difference in the production of these cytokines is closely linked to the development of CAWS-vasculitis. *The Journal of Immunology*, 2009, 183: 3417–3424.

Vasculitis syndrome is a collective term for diseases caused by vasculitis, which is defined as inflammation of the vascular wall (endothelium, tunica media, and adventitia) and its adjacent parts. In arteries and veins, vasculitis is characterized by the localized infiltration of inflammatory cells into the intravascular wall and its surroundings, accompanied by denaturation and necrosis. Many diseases, including Takayasu's disease, Wegener's granulomatosis, and Buerger's disease, are known to cause vasculitis. However, the cause of various clinical pathologies or groups of disorders brought about by vasculitis remains unknown. The techniques of molecular biology and genetic engineering are well established, and new technologies have been developed frequently in these fields. Using such technologies, the etiology and pathology of vasculitis is being clarified gradually.

Kawasaki disease was first reported by Dr. T. Kawasaki in 1967 and is also called acute febrile mucocutaneous lymph node syndrome (1). It is a disease characterized by fever continuing for 5 days or longer, hyperemia of bulbar conjunctiva in both eyes, strawberry tongue, and atypical rash; the cause of which is unknown. Systemic vasculitis develops in Kawasaki disease patients. In particular, vasculitis of the coronary artery as sequela is of concern (2). The coronary vasculitis develops further into coronary aneurysm. If the aneurysm is relatively small, it can be normalized within 1 or 2 years in most cases. However, a large aneurysm may result in occlusion by forming a thrombus, complicated with myocardial ischemia and myocardial disorders, and lead to sudden death because of myocardial infarction. In regard to this occasionally lethal vasculitis, although the incidence of coronary disorders has been on the decline because of recently introduced gammaglobulin therapy, neither the pathogenic mechanism nor therapeutic pharmacological mechanism is known (3, 4).

Murata and colleagues et al. (5–7) revealed that arteritis similar to coronary vasculitis, which is known as a sequela of Kawasaki disease, can be induced in mice by *Candida albicans*-derived substances in the forms of a KOH extract of *C. albicans* cell wall. Subsequently, *C. albicans* water-soluble fraction (CAWS)[3] was studied for its ability to induce vasculitis, and it was found to induce vasculitis at a higher rate than *C. albicans*-derived substances. The results indicated that CAWS is very useful for the analysis of the pathogenesis of this disease (8–15).

A deficiency of Bruton's tyrosine kinase (Btk) in humans causes serious sequela. This condition is known as X-linked agammaglobulinemia. Patients with X-linked agammaglobulinemia are vulnerable to infection, and administration of Ig is indicated (16). In mouse, the lack of Btk is called Xid (*xid*), and CBA/N mice have this genetic background (17).

CBA/J and CBA/N mice were differentiated from CBA/H mice, which were derived from DBA mice. In CBA/N mice, several phenomena caused by the lack of Btk have been reported. Btk is believed to be essential for B cell differentiation and maturation. In

*Laboratory for Immunopharmacology of Microbial Products, Tokyo University of Pharmacy and Life Sciences, Tokyo, Japan; †Laboratory of Genetic Resources, National Institute of Biomedical Innovation, Osaka, Japan; ‡National Institute of Infectious Diseases, Tokyo, Japan; and §Graduate School of Medicine and School of Medicine, Chiba University, Chiba, Japan

Received for publication August 6, 2008. Accepted for publication July 4, 2009.

The costs of publication of this article were defrayed in part by the payment of page charges. This article must therefore be hereby marked *advertisement* in accordance with 18 U.S.C. Section 1734 solely to indicate this fact.

[1] This work was partly supported by a grant-in-aid for Scientific Research from the Ministry of Education, Culture, Sports, Science, and Technology of Japan and the Promotion and Mutual Aid Corporation for Private Schools (Japan). This study was also supported by the Ministry of Health, Labour, and Welfare of Japan by a Grant for "Research on Regulatory Science of Pharmaceuticals and Medical Devices" and by the Program for Promotion of Basic and Applied Researches for Innovations in Bio-oriented Industry.

[2] Address correspondence and reprint requests to Dr. Naohito Ohno, Laboratory for Immunopharmacology of Microbial Products, Tokyo University of Pharmacy and Life Sciences, 1432-1 Horinouchi, Hachioji, Tokyo 192-0392, Japan. E-mail address: ohnonao@ps.toyaku.ac.jp

[3] Abbreviations used in this paper: CAWS, *Candida albicans* water-soluble fraction; Btk, Bruton's tyrosine kinase; EVG, Elastica-van-Gieson; MMP, matrix metalloprotease; PAF, platelet-activating factor; PAMP, pathogen-associated molecular pattern; TIMP1, tissue inhibitor of metalloproteinase 1.

www.jimmunol.org/cgi/doi/10.4049/jimmunol.0802484

particular, this enzyme is reported to participate in rearrangement of the L chain gene during pre-B cell differentiation into immature B cells. Consequently, few mature B cells exist in CBA/N mice, and their Ab-producing ability is decreased (18–20). Other effects of the lack of Btk include a decrease in NO production in macrophages, an increase in IL-12 production, and a decrease in IL-5 production from T cells (21, 22).

This study examined the ability of CAWS to induce vasculitis in CBA/N mice, histologically analyzed CBA/N and CAWS-vasculitis-resistant CBA/J mice, and compared the difference in cytokine responses and the inflammatory parameters between CBA/N and CAWS-vasculitis-resistant CBA/J mice. CAWS-vasculitis inhibitory factors were also analyzed.

Materials and Methods

Experimental animals

Male CBA/N and DBA/2 mice were acquired from Japan SLC. Male CBA/J mice were acquired from Charles River Japan. The animals were raised in a specific pathogen-free environment. Mice aged 5–14 wk were used in this study. All animal experiments in Tokyo University of Pharmacy and Life Sciences (TUPLS), and each of the experimental protocols was approved by the Committee of Laboratory Animal Experiments of TUPLS.

Fungi

C. albicans strain NBRC1385 was acquired from the National Institute of Technology and Evaluation Biological Resource Center, stored on Sabouraud agar medium (Difco) at 25°C, and subcultured once every 3 mo.

Preparation of CAWS

CAWS was prepared from *C. albicans* strain NBRC1385 in accordance with conventional methods. Culture was performed in 5 liters of C-limiting medium for 2 days at a rotating speed of 400 rpm while pumping in air at 27°C and 5 L/min. After culturing, an equal volume of ethanol was added, and after allowing to stand undisturbed overnight, the precipitate was recovered. This fraction was dissolved in 250 ml of distilled water, ethanol was added, and the solubilized fraction was allowed to stand undisturbed overnight. The precipitate was recovered and dried with acetone to obtain CAWS.

Administration schedule for induction of CAWS-vasculitis

CAWS (0 or 4 mg/mouse) was administered i.p. for 5 consecutive days to each mouse. At 28 days after CAWS injection, mice were sacrificed, and the hearts of the animals were fixed with 10% neutral formalin and prepared in paraffin blocks. Tissue sections were stained with H&E stain or Elastica-van-Gieson (EVG) stain.

Examination of IL-10 and endogenous matrix metalloproteinase (MMP) inhibitor (tissue inhibitor of metalloproteinase 1 (TIMP1)) mRNA expression levels in aorta by RT-PCR

The spleen and the aorta were resected from mice, frozen in liquid nitrogen, and immediately stored in Isogen (Nippon Gene). Each sample was homogenized with a homogenizer, and RNA was isolated by chloroform extraction. The total RNA level was determined by measuring OD using Nanodrop-ND1000. All total RNA were stored at −80°C or below.

Nuclease-free water was added to the total RNA along with oligo dT_{20} primer (Promega), and the reaction was conducted in a Thermal Cycler (Takara) at 70°C for 5 min. The product was cooled immediately by placing the reaction on ice for 5 min. Then, the following reagents were added: Moloney murine leukemia virus reverse transcriptase XL (Promega), PCR nucleotide mix (dNTP) (Promega), Moloney murine leukemia virus reverse transcriptase 5× reaction buffer, and nuclease-free water. The reverse transcriptase reaction was performed at 42°C for 60 min in a total volume of 25 μl/tube to obtain cDNA. The obtained cDNA was used as a template by adding PCR Master Mix (2×) (Promega), forward primer, reverse primer, and nuclease-free water, and heat denaturation was performed at 94°C for 2 min. One cycle consisted of heat denaturation at 94°C for 10 s, primer annealing at 55°C for 30 s, and elongation at 72°C for 1 min. Thirty cycles of this reaction were performed to obtain the PCR products. The primer sequences are shown as follows, all of which were purchased from Sigma-Genosys: IL-10 forward primer, 5′-ACCTGGTAGAAGTGTATGCCCCAGGCA-3′; IL-10 reverse primer, 5′-CTATGCAGTTGATGAAGATGTCAAA-3′; TIMP1 forward primer, 5′-ACTCGGACCTGGTCATAAGGGC-3′; TIMP1 reverse primer, 5′-AAGAAGCTGCAGGCACTGAT-3′; β-actin forward primer, 5′-TGGAATCCTGTGGCATCCTGAAAC-3′; and β-actin reverse primer, 5′-TAAAACGCAGCTCAGTAACAGTCCG-3′.

Comprehensive analysis of expressed gene by gene chip

We pooled total RNA from the spleens of three DBA/2 and two CBA/J mice for each strain after 21 days from the injection of CAWS. The probes labeled by cyanin3 and cyanin5 were hybridized with a DNA microarray (mouse 10K oligo chip; DNA Chip Consortium) on which 10,386 clones were spotted. After washing, fluorescence was measured using an array scanner. The fluorescence intensity of each spot was corrected by subtracting the background fluorescence intensity. Genes of signal intensity values <1000 were excluded because these may be detected nonspecifically. The microarray data was deposited to Gene Expression Omnibus (accession no. GSE16529; www.ncbi.nlm.nih.gov/geo/query/acc.cgi).

Spleen cell culture

The mice were euthanized by inhalation of CO_2, after which the spleen was excised. After teasing using a mesh in RPMI 1640 medium, the tissue was separated by centrifugation at 1200 rpm by 5 min, and the resulting cells were treated with Ammonium Chloride Potassium lysing buffer (8.20 g/L NH_4Cl, 1 g/L $KHCO_3$, and 37.2 mg/L EDTA 2Na). After two washes with RPMI 1640 medium, the spleen cells were counted to adjust the cell density and then used after being suspended in RPMI 1640 medium with 10% FCS. The spleen cells were adjusted to 5×10^6 in RPMI 1640 medium containing 10% FCS, and 500-μl aliquots were added to each well of a 48-well plate. After the addition of LPS (from *Escherichia coli* serotype 0111:B4; SIGMA), CpG (1668; 5′-TCCATGACGTTCCTGATGCT-3′; Sigma-Genosys), or tri-acylated lipoproteine (Pam_3-CSK_4), the cells were cultured for 48 h in a 5% CO_2 incubator at 37°C. The cytokine level of the culture supernatant was determined by ELISA as described below.

Measurement of IL-10 and TIMP1

IL-10 level was measured using a OPT_{EIA} IL-10 ELISA kit (BD Pharmingen), and the TIMP1 level was measured using a RayBio Mouse TIMP1 ELISA kit.

Measurement of IFN-γ

A 96-well ELISA plate (Nunc) was coated with rat anti-mouse IFN-γ mAb (BD Pharmingen) using 0.1 M $NaHCO_3$ (pH 8.2) and incubated overnight at 4°C. After washing with 0.05% Tween PBS (PBST), the Ab was blocked for 40 min at 37°C with 0.5% BSA-PBST (BPBST). This was followed by the addition of standards and samples (50 μl each), incubation for 40 min at 37°C, and six washes with PBST. Fifty microliters of a secondary Ab in the form of biotinylated rat anti-mouse IFN-γ (1/1000; BD Pharmingen) was then added, and after incubation for 40 min at 37°C and a wash with PBST, peroxidase-conjugated streptavidin (1/2000; BD Pharmingen) was added. This was followed by incubation for 40 min at 37°C and six washes with PBST. Subsequently, color was generated using peroxidase substrate (tetramethylbenzidine microwell peroxidase substrate system; Kirkegaard & Perry Laboratories). After termination of the reaction with 1 M phosphoric acid, absorbance (OD450/reference OD630) was measured. Recombinant mouse IFN-γ (BD Pharmingen) was used as the standard.

Measurement of IL-6

A 96-well ELISA plate (Nunc) was coated with rat anti-mouse IL-6 mAb (BD Pharmingen) using 0.1 M bicarbonate buffer (pH 9.5) and incubated overnight at 4°C. After washing with PBST, the Ab was blocked for 40 min at 37°C with BPBST. This was followed by the addition of standards and samples (50 μl each), incubation for 40 min at 37°C, and six washes with PBST. Fifty microliters of a secondary Ab in the form of biotinylated rat anti-mouse IL-6 (1/2000; BD Pharmingen) was then added, and after incubation for 40 min at 37°C and a wash with PBST, peroxidase-conjugated streptavidin (1/10,000; BD Pharmingen) was added. This was followed by incubation for 40 min at 37°C and six washes with PBST. Subsequently, 50 μl of peroxidase substrate (tetramethylbenzidine microwell peroxidase substrate system; Kirkegaard & Perry Laboratories) was added to generated color, and absorbance was measured as described previously. Recombinant mouse IL-6 (BD Pharmingen) was used as the standard.

Test for significant difference

Tests for significant differences in this study were performed using Student's *t* test, and values with $p < 0.05$ were judged significant.

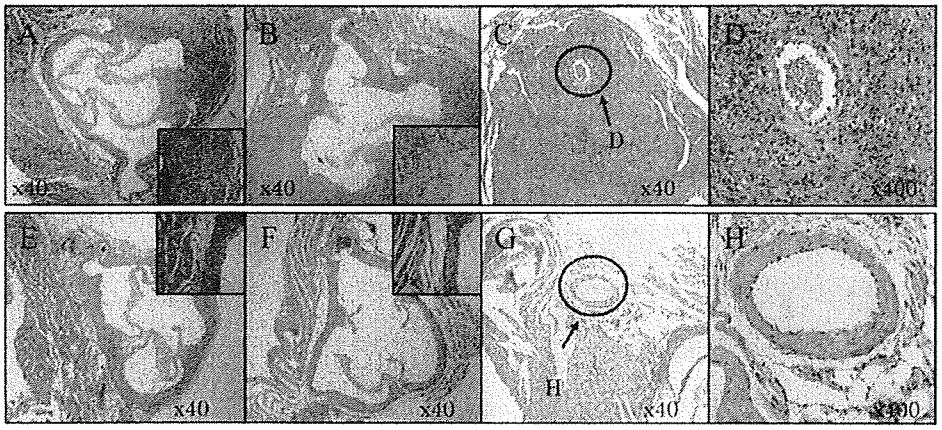

FIGURE 1. Histopathological findings of coronary arteries and aorta in CBA/N and CBA/J mice. CAWS (4 mg/mouse) was i.p. administered to CBA/N (*A–D*) and CBA/J (*E–H*) mice for 5 consecutive days. At 14 (*A* and *E*) and 28 (*B–D* and *F–H*) days after CAWS injections, mice were sacrificed and stained using H&E.

Results

Histological analysis of CAWS-vasculitis in CBA/J and CBA/N mice

Following the protocol for CAWS-vasculitis induction, CAWS was administered to CBA/J and CBA/N mice, and tissue slices of the beginning of aorta were prepared and stained with HE and EVG for observation. As a result, a 100% incidence of vasculitis was observed in the aorta and coronary artery of CBA/N mice (Fig. 1, *A–D*). This vasculitis in CBA/N mice developed 2 wk after the administration of CAWS. In contrast, no significant inflammatory changes were observed in the intima or adventitia of the aorta or the coronary artery in CBA/J mice (Fig. 1, *E–H*). EVG staining revealed injuries to the elastic fibers of CBA/N mice, which developed into CAWS-vasculitis, but similar injuries were not observed in CAWS-vasculitis-resistant CBA/J mice (Fig. 2).

cDNA microarray analysis of gene expression in spleen

To determine factors that participated in the onset of CAWS-vasculitis, genome-wide patterns of gene expression in challenged mice were examined using DNA microarrays. DBA/2 was only the strain in the present experiments that died because of CAWS-vasculitis. On the other hand, CBA/J mice showed the strongest resistance to CAWS-vasculitis among the inbred strains used in these experiments. To compare the difference in gene expression in the spleen at the time of vasculitis development between DBA/2 and CBA/J mice, a comprehensive analysis of the difference among strains was performed using the oligo-DNA microarrays.

As genes showing low expression in the hybridization detection system are not reliable, spots with a sum of cyanin3 and cyanin5 fluorescence intensities exceeding 1000 and having differences of ≧1.5 times were selected. According to these criteria, 271 genes were up-regulated in CBA/J mice, and 148 genes were up-regulated in DBA/2 mice. Genes with unknown function in the public database were filtered out. A list of differentially expressed genes was shown in Table I. In DBA/2 mice, the expression of inflammatory genes, such as *cathepsin G*, *myeloperoxidase*, *proteinase 3*, and *neutrophil elastase*, was increased, whereas in CBA/J mice, that of *TIMP1* was increased.

As described above, DBA/2 mice are the most sensitive strain to CAWS-vasculitis, and CBA/J is the most resistant. Many inflammatory as well as anti-inflammatory genes were differentially expressed between CBA/J and DBA/2 strains, suggesting that genes responsible for inflammation may play an important role for vasculitis. In this study, a third strain, CBA/N, which exhibits Btk deficiency and it is moderately sensitive to CAWS-vasculitis, was used, as shown in Figs. 1 and 2. At present, it was decided not to carry out microarray analysis using CBA/N because of its intermediate phenotype. However, this strain is superior for quantitative experiments, as shown later (Fig. 3).

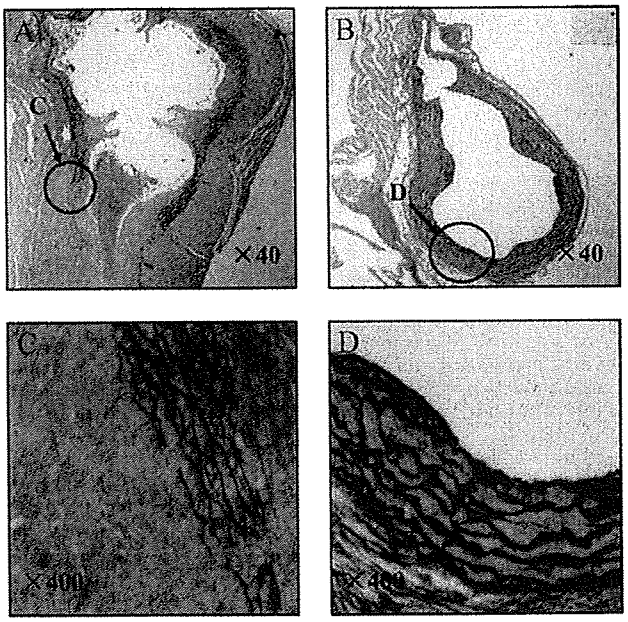

FIGURE 2. Histopathological findings of coronary arteries and aorta. CAWS (4 mg/mouse) was i.p. administered to CBA/N (*A* and *C*) and CBA/J (*B* and *D*) mice for 5 consecutive days. At 28 days after CAWS injections, mice were sacrificed and stained with EVG stain.

Blood cytokine production in the initial phase after CAWS administration

CBA/J is the only mouse strain resistant to CAWS-vasculitis among the inbred mouse strains studied so far. It was reported previously that anti-inflammatory cytokine IL-10 (23) production is increased in CBA/J mice (11). Therefore, the serum IL-10 level was measured in CBA/J and CBA/N mice after administration of CAWS (4 mg in PBS/mouse), along with the production of TIMP1, an endogenous matrix metalloprotease inhibitor, the gene expression level of which was found to be increased in the cDNA microarray analysis.

In CBA/J mice, high levels of IL-10 were produced 1 h after CAWS administration. In contrast, IL-10 production was hardly detected in CBA/N mice (Fig. 3*A*). In CBA/J mice, TIMP1 showed high levels 4 h after CAWS administration, and it continued to increase even at 10 h after CAWS administration. On the other

Table I. *Genes differentially expressed in CBA/J and DBA/2 splenocytes at day 21*[a]

Gene Name	$\log_2$ Ratio	UniGene
Myeloperoxidase	3.04	Mm.4608
Neutrophilic granule protein	2.79	Mm.2827
TNF (ligand) superfamily, member 12	2.73	Mm.8983
S100 calcium-binding protein A9 (calgranulin B)	2.58	Mm.2128
Cathelicidin antimicrobial peptide	2.50	Mm.21855
Peptidoglycan recognition protein	2.47	Mm.3834
Cathepsin G	2.30	Mm.4858
S100 calcium-binding protein A8 (calgranulin A)	2.27	Mm.21567
GATA-binding protein 1	2.05	Mm.1344
CD24a Ag	2.02	Mm.6417
Hemoglobin Z, β-like embryonic chain	1.90	Mm.196718
Lipocalin 2	1.89	Mm.9537
Carbonic anhydrase 1	1.82	Mm.3471
Chemokine (C-X-C motif) ligand 7	1.62	Mm.157750
Fibronectin 1	1.51	Mm.193099
Chemokine (C-X-C motif)ligand 4	1.50	Mm.23905
Neutrophil elastase	1.39	Mm.271137
Proteinase 3	1.35	Mm.2364
Aminolevulinate, δ-, dehydratase	1.34	Mm.6988
TNF, α-induced protein 2	1.28	Mm.4348
Chemokine (C-X-C motif) receptor 4	1.18	Mm.1401
C-type lectin-like receptor 2	1.12	Mm.30700
IFN-stimulated protein	1.11	Mm.19029
Chemokine(C-X-C motif) ligand 5	0.99	Mm.4660
Chemokine (C-C motif) receptor 1-like 1	0.95	Mm.57056
IL-12R, β1	0.95	Mm.731
TGF-β1-induced transcript 4	0.94	Mm.20927
TIMP1	−5.44	Mm.8245
Insulin 1	−5.20	Mm.46269
Chemokine (C-C motif) receptor 8	−4.89	Mm.8000
IL-8R, β	−4.43	Mm.234466
Carboxyl ester lipase	−4.43	Mm.4349
Carboxypeptidase B1 (tissue)	−4.30	Mm.34692
Regenerating islet-derived 2	−4.25	Mm.46360
Pancreatic lipase-related protein 2	−4.14	Mm.1230
Glycoprotein hormones, α subunit	−4.10	Mm.1361
Serine protease inhibitor, Kazal type 3	−4.04	Mm.272
Elastase 1, pancreatic	−3.97	Mm.2131
Regenerating islet-derived 1	−3.97	Mm.142731
Protease, serine, 18	−3.94	Mm.3944
Pancreatic lipase-related protein 1	−3.66	Mm.10753
Chemokine(C-X-C motif) ligand 11	−3.33	Mm.131723
Cholinergic receptor, nicotinic, β-polypeptide 1	−2.97	Mm.86425
Elastase 2	−2.92	Mm.21925
Pancreatitis-associated protein	−2.71	Mm.2553
Chymotrypsin-like	−2.70	Mm.2745
Inhibitor of κB kinase γ	−2.60	Mm.12967
Islet neogenesis-associated protein-related protein	−2.53	Mm.33691
Protease, serine, 21	−2.35	Mm.86657
TNFR superfamily, member 12a	−1.85	Mm.28518
Inter-α trypsin inhibitor, heavy chain 1	−1.75	Mm.3227
Carboxipeptidase A1	−1.64	Mm.25377
Thioredoxin 1	−1.31	Mm.260618

[a] The genes with negative ratio values are abundant in the CBA/J mice, whereas genes with positive ratio values are abundant in the DBA/2. The microarray data was deposited to Gene Expression Omnibus (accession no. GSE16529; www.ncbi.nlm.nih.gov/geo/query/acc.cgi).

hand, in CBA/N mice, TIMP1 showed high levels 4 h after CAWS administration similar to CBA/J mice, but it decreased at 10 h after CAWS administration (Fig. 3*B*).

Gene expression levels in the spleen and the aorta in the initial phase after CAWS administration

The gene expression levels of anti-inflammatory cytokines were compared in the initial phase after CAWS administration in CBA/J and CBA/N mice. CAWS (4 mg/0.2 ml PBS) was administered i.p., and the effect was examined using RT-PCR to measure IL-10 and TIMP1 gene expression levels in the spleen and the aorta 1 and 3 h after the administration (Fig. 4). β-Actin was used as the internal standard and for correcting the expression level of each sample.

IL-10 gene expression in spleen cells at 1 and 3 h after CAWS administration was higher in CBA/J mice than in CBA/N mice. In particular, high expression levels were observed 1 h after CAWS

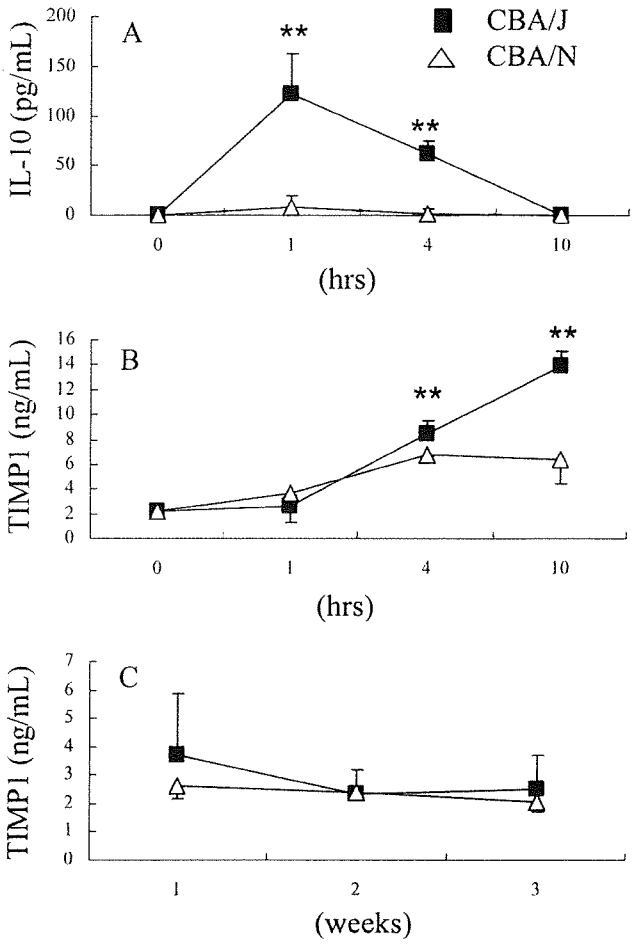

FIGURE 3. Serum IL-10 and TIMP1 leads to CAWS-injected CBA/J and CBA/N mice. Serum was collected from CBA/J and CBA/N mice i.p. injected with CAWS (4 mg/mouse) at various time points (six animals per group). IL-10 (*A*) and TIMP1 (*B*; after 0, 1, 4, 10 hours of CAWS administration, *C*; after 1, 2, 3 wk of CAWS administration) production was measured using ELISA. *, $p < 0.05$; **, $p < 0.001$ (vs 0 h).

administration. It was also observed that TIMP1 gene expression was increased in CBA/J mice after CAWS administration. However, contrary to the expectation, a particularly high expression was observed in CBA/N mice 3 h after CAWS administration (Fig. 4, *A* and *C*).

A markedly higher expression level of IL-10 gene in aorta cells of CBA/J mice was noted 1 h after CAWS administration. The IL-10 gene expression level in CBA/N mice was lower than that in CBA/J mice, but the TIMP1 gene expression level was similar in both strains before and after the administration of CAWS (Fig. 4, *B* and *D*).

Blood cytokine production in the late phase after CAWS administration

It was reported that CAWS-vasculitis begins to develop ~1 wk after CAWS administration (10). Using ELISA, serum cytokine production was measured in the late phase after CAWS administration (4 mg/0.2 ml PBS) when the vasculitis was thought to have developed (Fig. 3*C*).

IL-10 production was not observed in either CBA/J or CBA/N mice in the late phase after CAWS administration (data not shown). After 1 wk of CAWS administration, TIMP1 production in CBA/J mice tended to be higher but not to a significant degree.

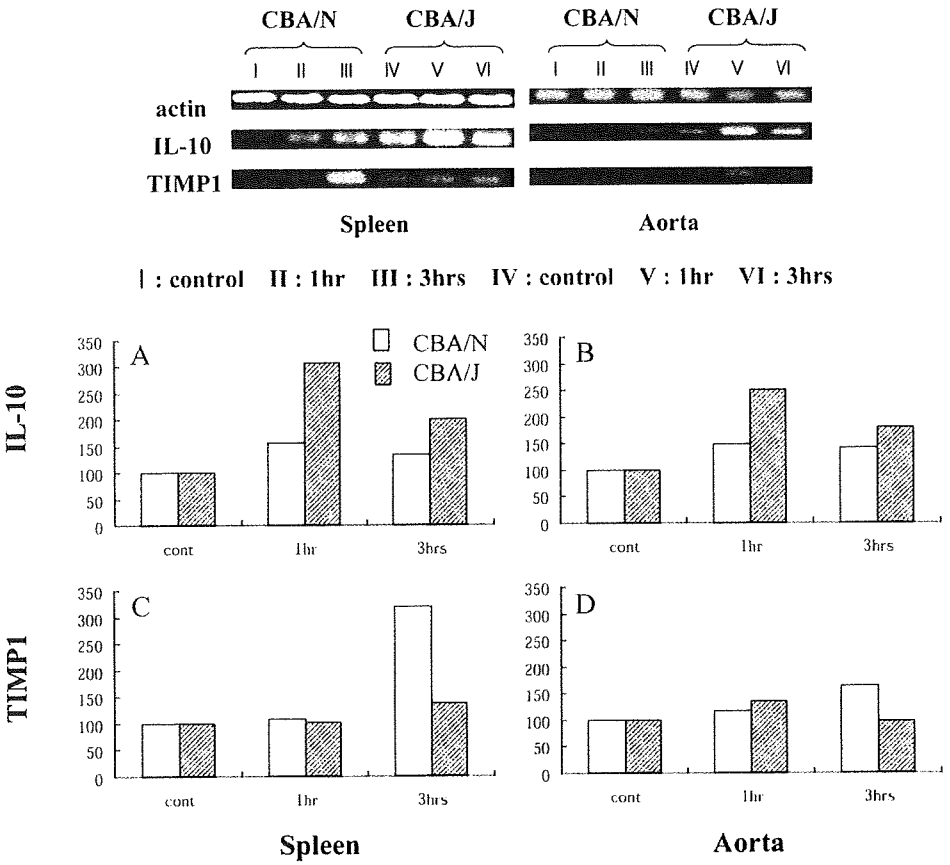

FIGURE 4. Semiquantitative analysis of IL-10 and TIMP1 mRNA expression ratios relative to actin in the spleen and aorta. Total RNA was isolated from the spleen and the aorta of CBA/J and CBA/N mice i.p. injected with CAWS (0 or 4 mg/mouse) at various time points. After the reverse transcriptase reaction was performed, each gene expression level was measured by semiquantitative PCR. Actin mRNA expression was also measured as an internal control and used for the normalized of target genes expression levels. *A*, IL-10 mRNA expression level in the spleen; *B*, IL-10 mRNA expression level in the aorta; *C*, TIMP1 mRNA expression level in the spleen; and *D*, TIMP1 mRNA expression level in the aorta.

TIMP1 production in CBA/J mice was not different from that in CBA/N mice after 2 or 3 wk of CAWS administration.

Gene expression in the spleen and the aorta in late phase after CAWS administration

IL-10 and TIMP1 gene expression levels were compared in the spleen and the aorta of CBA/J and CBA/N mice during the vasculitis-forming phase after CAWS administration. CAWS (4 mg/0.2 ml PBS) was administered i.p. for 5 consecutive days, and IL-10 and TIMP1 gene expression levels were examined by RT-PCR in the spleen and the aorta 2 and 4 wk after the last administration.

High IL-10 gene expression levels were observed in both the spleen and the aorta of CBA/J mice 2 wk after CAWS administration (Fig. 5). On the other hand, no IL-10 gene expression was observed in CBA/N mice. High TIMP1 gene expression was noted in the aorta of CBA/J mice 2 and 4 wk after CAWS administration. In addition, in the late phase after CAWS administration, the gene expression level in the spleen and the aorta showed a similar pattern.

Cytokine production in spleen cells of CBA/J and CBA/N mice after stimulation with pathogen-associated molecular patterns (PAMP)

Previous studies have indicated that when spleen cells of DBA/2 and CBA/J mice in which vasculitis had been induced by CAWS were cultured with CAWS the production of non-anti-inflammatory cytokines but not inflammatory cytokines was observed in DBA/2 mice, whereas the production of non-inflammatory cytokines but not anti-inflammatory cytokine IL-10 was observed in CBA/J mice (11). Therefore, the production of IL-10 and inflammatory cytokines IL-6 and IFN-γ was studied in CBA/J and CBA/N mice. The following PAMP were used: LPS, a Gram-negative bacterial cell wall component recognized by TLR4; PAM3, which is recognized by TLR2; and CpG, a synthetic oligodeoxynucleotide recognized by TLR9.

Upon stimulation with these PAMP recognized by respective TLR, the production of a large amount of IL-10 was observed in the spleen cells of CBA/J mice, which show resistance to CAWS-vasculitis. The production of IL-6 and IFN-γ was hardly observed in the spleen cells of CBA/J mice. On the other hand, in the spleen cells of CBA/N mice, which are sensitive to CAWS-vasculitis, the production of IL-6 and IFN-γ but not IL-10 was observed (Fig. 6).

Acute lethal activity in CAWS-administered mice

Other than its vasculitis-inducing activity, CAWS is known for its acute lethal activity after i.v. administration (12, 13). As a positive control, a closed colony of ICR mice was used, in which ~100% acute lethal activity is observed. A 200-μg acute lethal dose of CAWS was administered to the closed-colony ICR mice, in addition to 400 μg of CAWS, which is double that amount, through the caudal vein of the mice.

The acute lethal activity of CAWS was clearly observed in vasculitis-resistant CBA/J mice. CBA/J mice showed reduced movement ~5 min after CAWS administration and shock status ~15 min after administration. Almost all the mice died within 25 min after administration. In contrast, no acute lethal activity was observed in vasculitis-sensitive CBA/N mice, and acute lethal activity was also not observed in DBA/2 mice that develop severe vasculitis (Table II).

Discussion

Kawasaki disease induces the development of systemic vasculitis. In particular, the vasculitis that develops in the coronary artery

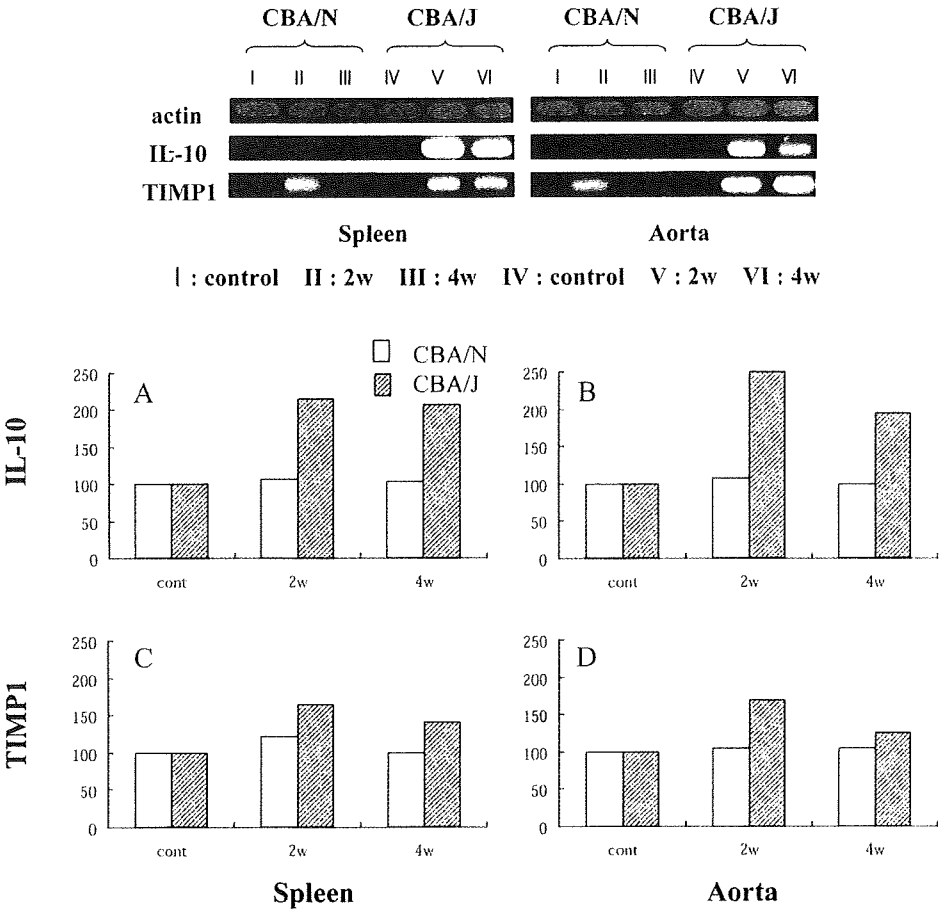

FIGURE 5. Semiquantitative analysis of IL-10 and TIMP1 mRNA expression ratios relative to actin in the spleen and the aorta. Total RNA was isolated from the spleen and the aorta of CBA/J and CBA/N mice i.p. injected with CAWS (0 or 4 mg/mouse) at various time points. After the reverse transcriptase reaction was performed, each gene expression level was measured by semiquantitative PCR. Actin mRNA expression level was also measured as an internal control and used for the normalized of target genes expression levels. *A*, IL-10 mRNA expression level in the spleen; *B*, IL-10 mRNA expression level in the aorta; *C*, TIMP1 mRNA expression level in the spleen; and *D*, TIMP1 mRNA expression level in the aorta.

sometimes becomes lethal, and thus, elucidation of the mechanisms underlying its pathogenesis and therapy is clinically important. According to Murata and colleagues (5–7), when CAWS is i.p. administered daily, vasculitis in the coronary artery, similar to that in Kawasaki disease, can be induced at a high rate. Although the vasculitis-inducing activity of CAWS has been studied in various inbred mouse strains, it was revealed for the first time that CAWS-vasculitis can be induced in Btk-deficient CBA/N mice (Figs. 1 and 2). Analysis of serial sections of the aorta stained with H&E suggested that the vasculitis in CBA/N mice was mild compared with that in DBA/2 mice, because aortic stenosis was mild and no reduction in survival rate was observe after CAWS administration (10, 14). Previous studies have shown that elastic fiber injury occurs in the aorta close to the beginning of the coronary artery in mice that develop CAWS-vasculitis (10). A similar phenomenon was observed in CBA/N mice as well. Because such a phenomenon was not observed in CAWS-vasculitis-resistant CBA/J mice, a rupture of the elastic fibers in CBA/N mice was thought to be attributable to CAWS-vasculitis. The aorta is an elastic-type artery, and this elasticity is due to the formation of a substantial elastic layer in the tunica media. The upper part of the aorta where CAWS-vasculitis occurs is particularly rich in elastic fibers. Therefore, the present observation that injury occurs in the aortic elastic fibers in CBA/N mice as a result of CAWS-vasculitis is an important finding for further analysis of CAWS-vasculitis in the future.

CBA/J mice showed resistance to CAWS-vasculitis. To the best of our knowledge, no inbred mouse strain, except for CBA/J, is resistant to CAWS-vasculitis. Therefore, further analysis of resistance to CAWS-vasculitis in CBA/J mice is considered to be important not only for the elucidation of the pathogenic mechanism of CAWS-vasculitis but also for the development of a therapeutic model. On the other hand, DBA/2 mice develop severe vasculitis following CAWS administration, and this vasculitis is fatal. No other strains of mice, except for DBA/2, showed fatal CAWS-vasculitis. To determine the factors that participated in the onset of CAWS-vasculitis, mRNA expression in the splenocytes from DBA/2 and CBA/J mice was examined using a microarray technique. High expression levels of mRNA such as myeloperoxidase, cathepsin G, neutrophil elastase, and proteinase 3 were recognized in DBA/2 mice. These proteins are well-known markers of neutrophils and correlate with inflammation.

TIMP1 was suggested to be one of the most important factors in the inhibition of CAWS-vasculitis in the results of the microarray analysis (Table I). TIMP1 is known to be a MMP-specific endogenous inhibitor. Contrary to expectation, temporarily high levels of TIMP1 were observed in CBA/J mice (Fig. 3). It was reported that there was no correlation between blood TIMP and MMP production levels and disease severity in multiple patients with Kawasaki disease, and an imbalance of these levels contributed to the development of vasculitis (24, 25). It was also suggested that the imbalance of TIMP and MMP is a factor contributing to the development of vasculitis. MMP was reported to be involved in vasculitis remodeling and the formation of vasculitis in Kawasaki disease (26). Therefore, further studies may be necessary to examine not only TIMP levels per se but also its production level relative to MMP.

The gene expression levels of IL-10 and TIMP1 in spleen and aortic root were examined at early and late stages of CAWS-vasculitis (Figs. 4 and 5). In the late stage (2–4 wk after CAWS

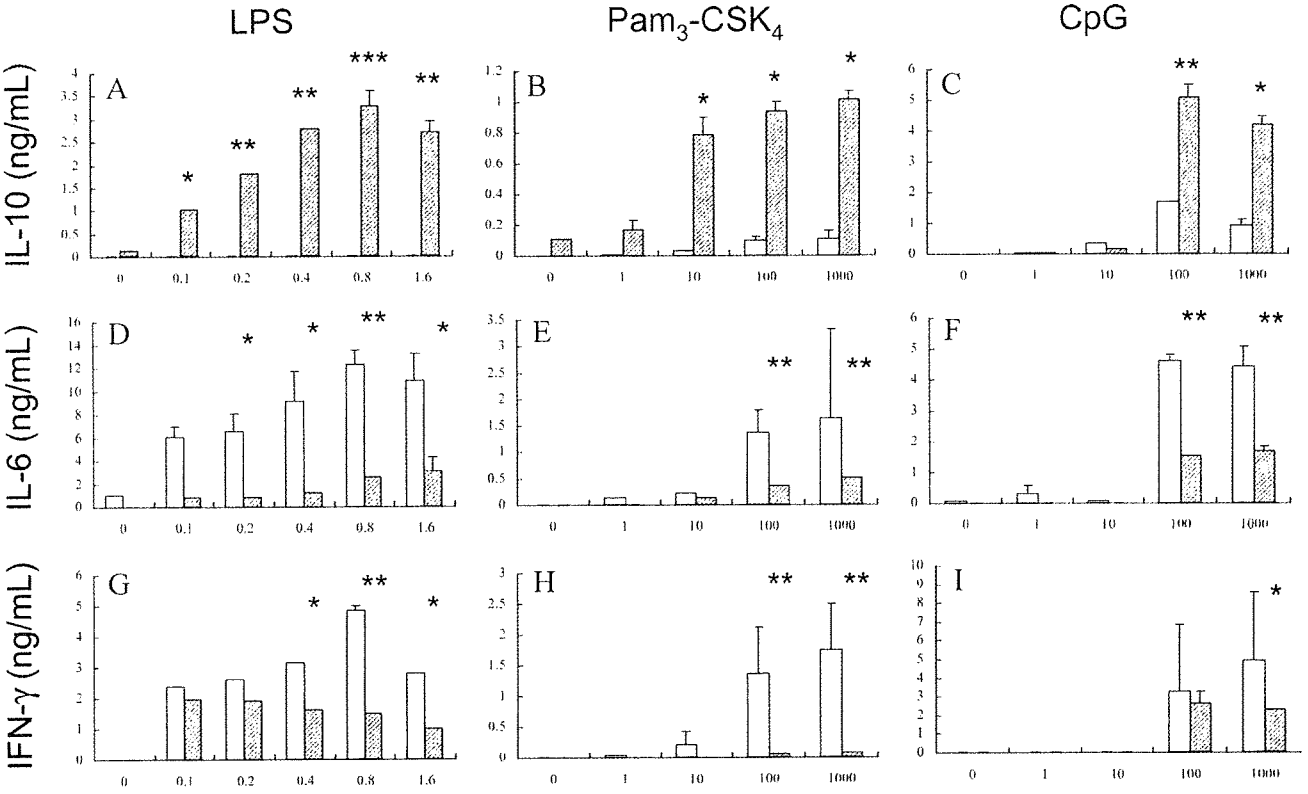

FIGURE 6. Cytokine production in culture supernatants of splenocytes from CBA/J and CBA/N mice stimulated with LPS, PAM_3-CSK_4, and CpG-oligodeoxynucleotide. Splenocytes were collected from CBA/J and CBA/N mice (four animals per group). Prepared splenocytes were cultured with LPS (0, 0.1, 0.2, 0.4, 0.8, or 1.6 μg/ml, *A*, *D*, *G*), PAM_3-CSK_4 (0, 1, 10, 100, or 1000 ng/ml, *B*, *E*, *H*), or CpG-ODN (0, 1, 10, 100, or 1000 nM, *C*, *F*, *I*) for 48 h at an initial density of 5×10^6 cells/ml. The culture supernatants were collected and measured for IL-10 (*A–C*), IL-6 (*D–F*), and IFN-γ (*G–I*) levels using ELISA. □, CBA/N; ▨, CBA/J. *, $p < 0.05$; **, $p < 0.001$ (vs blank).

administration), CAWS-vasculitis had developed, and the infiltration of leukocytes in CBA/N mice was significant. In contrast, leukocyte infiltration into the aortic root was scarce in CBA/J mice (Figs. 1 and 2). It was of interest that both IL-10 and TIMP1 were highly expressed in the aortic root of CBA/J mice. IL-10 acts as anti-inflammatory, and TIMP1 protects tissues from proteases; thus, the expression of both genes concomitantly protects the tissue from inflammation. In the case of CBA/N mice, TIMP1 was expressed weakly, but no IL-10 expression could be detected. The anti-inflammatory system of the aortic root could be weak. Of interest, gene expression in the aortic root and spleen are similar for both genes, suggesting that inflammatory and/or anti-inflammatory states may not be local but systemic. In the early stage of CAWS-vasculitis, when leukocyte infiltration is scarcely induced in both strains of mice, both IL-10 and TIMP1 expression levels were also high in CBA/J mice. From both the results of early and late stages, it was suggested that cells expressing IL-10 and TIMP1 may not be infiltrating inflammatory cells but resident cells of the aortic tissue, such as endothelial cells, fibroblasts, and smooth muscle cells, as well as resident macrophages. However, precise characterization of the cells expressing anti-inflammatory cytokines and molecules was not performed in this study.

Table II. *Acute lethal toxicity of CAWS i.v. administrated mice*[a]

	CBA/J	CBA/N	DBA/2	ICR
200 μg/mouse	4/5	0/5	0/5	5/5
400 μg/mouse	5/5	0/5	0/5	5/5

[a] The acute lethal toxicity of CAWS was monitored after i.v. administration to ICR mice and observing the mice that died within 1 h after administration.

Stimulation of spleen cells of both CBA/J and CBA/N mice with various PAMP revealed high IL-10 production in the spleen cells of CBA/J mice (Fig. 6). It is known that PAMP are mainly recognized by TLR on the cell surface (27). On the other hand, IL-10 was barely produced in the spleen cells of CBA/N mice, whereas the production of inflammatory cytokines IL-6 and IFN-γ was observed. Such cytokine responses are thought to be a factor contributing to the development of CAWS-vasculitis in CBA/N mice. As described earlier, CBA/N mice have a genetic background lacking Btk compared with wild-type CBA/J mice. Therefore, it was strongly suggested that Btk is involved in the difference in IL-10 production between the two mouse strains.

As a result of studies on acute lethal activity after CAWS administration in various inbred mouse strains, in which vasculitis-inducing activity is obvious, this study observed acute lethal activity in vasculitis-resistant CBA/J mice. In contrast, vasculitis-sensitive CBA/N and DBA/2 mice did not show acute lethal activity (Table II). Although the mechanism underlying the development of acute lethal activity has not been completely elucidated, the fact that CAWS is a mannoprotein-β-glucan complex suggests that the complement lectin pathway is involved (28). It was also speculated that in accordance with the activation of the complement lectin pathway by CAWS, anaphylatoxin production and subsequent production of platelet-activating factor (PAF) are activated. PAF is suggested to play an important role in the shock observed when yeast mannan is administered (29). It was reported that PAF receptor induces the production of IL-10 (30–34). However, it remains unknown whether Btk, which is the genetic

difference between CBA/J and CBA/N mice, affects these pathways or not.

From these results, CBA/J mice are thought to be resistant to vasculitis because the inhibitory pathway, including IL-10, is easily induced not only by CAWS but also by various ligands.

Acknowledgments

We thank Hiroki Sankawa for excellent technical assistance.

Disclosures

The authors have no financial conflict of interest.

References

1. Kawasaki, T., and F. Kousaki. 1967. Febrile oculo-oro-cutaneo-acrodesquamatous syndrome with or without acute nonsuppurative cervical lymphadenitis in infancy and childhood: clinical observations of 50 cases (in Japanese). *Jpn. J. Allergy* 16: 178–222.
2. Newburger, J. W., M. Takahashi, M. A. Gerber, M. H. Gewitz, L. Y. Tani, J. C. Burns, S. T. Shulman, A. F. Bolger, P. Ferrieri, R. S. Baltimore, et al. 2004. Diagnosis, treatment, and long-term management of Kawasaki disease: a statement for health professionals from the Committee on Rheumatic Fever, Endocarditis and Kawasaki Disease, Council on Cardiovascular Disease in the Young, American Heart Association. *Circulation* 110: 2747–2771.
3. Newburger, J. W., M. Takahashi, A. S. Beiser, J. C. Burns, J. Bastian, K. J. Chung, S. D. Colan, C. E. Duffy, D. R. Fulton, and M. P. Glode. 1991. A single intravenous infusion of gammaglobulin as compared with four infusions in the treatment of acute Kawasaki syndrome. *N. Engl. J. Med.* 324: 1633–1639.
4. Furusho, K., T. Kamiya, H. Nakano, N. Kiyosawa, K. Shinomiya, T. Hayashudera, T. Tamura, O. Hirose, Y. Manabe, and T. Yokoyama. 1984. High-dose intravenous gammaglobulin for Kawasaki disease. *Lancet* 2: 1055–1058.
5. Murata, H., H. Iijima, S. Naoe, T. Atobe, T. Uchiyama, and S. Arakawa. 1987. The pathogenesis of experimental arteritis induced by *Candida* alkali extract in mice. *Jpn. J. Exp. Med.* 57: 305–313.
6. Murata, H., and S. Naoe. 1987. Experimental *Candida*-induced arteritis in mice—relation to arteritis in Kawasaki disease. *Prog. Clin. Biol. Res.* 250: 523.
7. Takahashi, K., T. Oharaseki, M. Wakayama, Y. Yokouchi, S. Naoe, and H. Murata. 2004. Histopathological features of murine systemic vasculitis caused by *Candida albicans* extract—an animal model of Kawasaki Disease. *Inflamm. Res.* 53: 72–77.
8. Ohno, N. 2008. A murine model of vasculitis induced by fungal polysaccharide. *Cardiovasc. Hematol. Agents Med. Chem.* 6: 44–52.
9. Ohno, N. 2006. Models of Kawasaki disease. *Drug Discov. Today Dis. Models* 3: 83–89.
10. Hirata, N., K. Ishibashi, S. Ohta, S. Hata, H. Shinohara, M. Kitamura, N. Miura, and N. Ohno. 2006. Histopathological examination and analysis of mortality in DBA/2 mouse vasculitis induced with CAWS, a water-soluble extracellular polysaccharide fraction obtained from *Candida albicans*. *Yakugaku Zasshi* 126: 643–650.
11. Nagi-Miura, N., Y. Shingo, Y. Adachi, A. Ishida-Okawara, T. Oharaseki, K. Takahashi, S. Naoe, K. Suzuki, and N. Ohno. 2004. Induction of coronary arteritis with administration of CAWS (*Candida albicans* water-soluble fraction) depending on mouse strains. *Immunopharmacol. Immunotoxicol.* 26: 527–543.
12. Kurihara, K., N. N. Miura, M. Uchiyama, N. Ohno, Y. Adachi, M. Aizawa, H. Tamura, S. Tanaka, and T. Yadomae. 2000. Measurement of blood clearance time by Limulus G test of *Candida*-water soluble polysaccharide fraction, CAWS, in mice. *FEMS Immunol. Med. Microbiol.* 29: 69–76.
13. Kurihara, K., Y. Shingo, N. N. Miura, S. Horie, Y. Usui, Y. Adachi, T. Yadomae, and N. Ohno. 2003. Effect of CAWS, a mannoprotein-β-glucan complex of *Candida albicans*, on leukocyte, endothelial cell, and platelet functions in vitro. *Biol. Pharm. Bull.* 26: 233–240.
14. Nagi-Miura, N., T. Harada, H. Shinohara, K. Kurihara, Y. Adachi, A. Ishida-Okawara, T. Oharaseki, K. Takahashi, S. Naoe, K. Suzuki, and N. Ohno. 2006. Lethal and severe coronary arteritis in DBA/2 mice induced by fungal pathogen, CAWS, *Candida albicans* water-soluble fraction. *Atherosclerosis* 186: 310–320.
15. Ishida-Okawara, A., N. Nagi-Miura, T. Oharaseki, K. Takahashi, A. Okumura, H. Tachikawa, S. Kashiwamura, H. Okamura, N. Ohno, H. Okada, et al. 2007. Neutrophil activation and arteritis induced by *C. albicans* water-soluble mannoprotein-β-glucan complex (CAWS). *Exp. Mol. Pathol.* 82: 220–226.
16. Kanegane, H., K. Nomura, T. Futatani, and T. Miyawaki. 2002. Intravenous immunoglobulin replacement therapy in X-linked agammaglobulinemia (in Japanese; includes abstract). *Jpn. J. Clin. Immun.* 25: 337–343.
17. Berning, A. K., E. M. Eicher, W. E. Paul, and I. Scher. 1980. Mapping of the X-linked immune deficiency mutation (*xid*) of CBA/N mice. *J. Immunol.* 124: 1875–1877.
18. Cancro, M. P., A. P. Sah, S. L. Levy, D. M. Allman, M. R. Schmidt, and R. T. Woodland. 2001. *xid* mice reveal the interplay of homeostasis and Bruton's tyrosine kinase-mediated selection at multiple stages of B cell development. *Int. Immunol.* 13: 1501–1514.
19. Middendorp, S., G. M. Dingjan, A. Maas, K. Dahlenborg, and R. W. Hendriks. 2003. Function of Bruton's tyrosine kinase during B cell development is partially independent of its catalytic activity. *J. Immunol.* 171: 5988–5996.
20. Satterthwaite, A. B., and O. N. Witte. 2000. The role of Bruton's tyrosine kinase in B cell development and function: a genetic perspective. *Immunol. Rev.* 175: 120–127.
21. Mukhopadhyay, S., M. Mohanty, A. Mangla, A. George, V. Bal, S. Rath, and B. Ravindran. 1999. Bruton's tyrosine kinase deficiency in macrophages inhibits nitric oxide generation leading to enhancement of IL-12 induction. *J. Immunol.* 163: 1786–1792.
22. Koike, M., Y. Kikuchi, A. Tominaga, S. Takaki, K. Akagi, J. Miyazaki, K. Yamamura, and K. Takatsu. 1995. Defective IL-5-receptor-mediated signaling in B cells of X-linked immunodeficient mice. *Int. Immunol.* 7: 21–30.
23. Moore, K. W., R. de Waal Malefyt, R. L. Coffman, and A. O'Garra. 2001. Interleukin-10 and the interleukin-10 receptor. *Annu. Rev. Immunol.* 19: 683–765.
24. Senzaki, H., S. Masutani, J. Kobayashi, T. Kobayashi, H. Nakano, H. Nagasaka, N. Sasaki, H. Asano, S. Kyo, and Y. Yokote. 2004. Circulating matrix metalloproteinases and their inhibitors in patients with Kawasaki disease. *Circulation* 104: 860–863.
25. Chua, P. K., M. E. Melish, Q. Yu, R. Yanagihara, K. S. Yamamoto, and V. R. Nerurkar. 2003. Elevated levels of matrix metalloproteinase 9 and tissue inhibitor of metalloproteinase 1 during the acute phase of Kawasaki disease. *Clin. Diagn. Lab. Immunol.* 10: 308–314.
26. Gavin, P. J., S. E. Crawford, S. T. Shulman, F. L. Garcia, and A. H. Rowley. 2003. Systemic arterial expression of matrix metalloproteinases 2 and 9 in acute Kawasaki disease. *Arterioscler. Thromb. Vasc. Biol.* 23: 576–581.
27. Jefferies, C. A., and L. A. O'Neill. 2004. Bruton's tyrosine kinase (Btk)—the critical tyrosine kinase in LPS signalling? *Immunol. Lett.* 92: 15–22.
28. Shinohara, H., N. Nagi-Miura, K. Ishibashi, Y. Adachi, A. Ishida-Okawara, T. Oharaseki, K. Takahashi, S. Naoe, K. Suzuki, and N. Ohno. 2006. β-Mannosyl linkages negatively regulate anaphylaxis and vasculitis in mice, induced by CAWS, fungal PAMPs composed of mannoprotein-β-glucan complex secreted by *Candida albicans*. *Biol. Pharm. Bull.* 29: 1854–1861.
29. Mikami, T., K. Fukushi, M. Ishitani, K. Ishitani, S. Suzuki, and M. Suzuki. 1994. Induction of platelet-activating factor in mice by intravenous administration of a neutral fraction of bakers' yeast mannan. *Lipids* 26: 1404–1407.
30. Zhang, Q., N. Mousdicas, Q. Yi, M. Al-Hassani, S. D. Billings, S. M. Perkins, K. M. Howard, S. Ishii, T. Shimizu, and J. B. Travers. 2005. Staphylococcal lipoteichoic acid inhibits delayed-type hypersensitivity reactions via the platelet-activating factor receptor. *J. Clin. Invest.* 115: 2855–2861.
31. Pei, Y., L. A. Barber, R. C. Murphy, C. A. Johnson, S. W. Kelley, L. C. Dy, R. H. Fertel, T. M. Nguyen, D. A. Williams, and J. B. Travers. 1998. Activation of the epidermal platelet-activating factor receptor results in cytokine and cyclooxygenase-2 biosynthesis. *J. Immunol.* 161: 1954–1961.
32. Dy, L. C., Y. Pei, and J. B. Travers. 1999. Augmentation of ultraviolet B radiation-induced tumor necrosis factor production by the epidermal platelet-activating factor receptor. *J. Biol. Chem.* 274: 26917–26921.
33. Southall, M. D., J. S. Isenberg, H. Nakshatri, Q. Yi, Y. Pei, D. F. Spandau, and J. B. Travers. 2001. The platelet-activating factor receptor protects epidermal cells from tumor necrosis factor (TNF) α and TNF-related apoptosis-inducing ligand-induced apoptosis through an NF-κB-dependent process. *J. Biol. Chem.* 276: 45548–45554.
34. Walterscheid, J. P., S. E. Ullrich, and D. X. Nghiem. 2002. Platelet-activating factor, a molecular sensor for cellular damage, activates systemic immune suppression. *J. Exp. Med.* 195: 171–179.

Color-coded real-time cellular imaging of lung T-lymphocyte accumulation and focus formation in a mouse asthma model

Akihiro Hasegawa, PhD,[a,c,d] Katsuhiro Hayashi, MD,[d] Hiroyuki Kishimoto, MD, PhD,[d] Meng Yang, MD, PhD,[d] Soichi Tofukuji, MS,[a] Kazuo Suzuki, PhD,[a] Hiroshi Nakajima, MD, PhD,[b] Robert M. Hoffman, PhD,[d,e] Mutsunori Shirai, MD, PhD,[c] and Toshinori Nakayama, MD, PhD[a] *Chiba and Ube, Japan, and San Diego, Calif*

Background: A critical role for $CD4^+T_H2$ cells in the pathogenesis of acute asthma has been demonstrated in the studies of human asthma as well as of animal models of asthma. T_H2-cell migration into the lung is crucial for the initiation of asthma phenotype, but the dynamics of this process are poorly understood because it has been difficult to visualize this process.

Objective: Our aim was to image the cellular dynamics of the migration of T_H2 cells into the lung of living animals in a mouse model of asthma and identify the cellular processes required for the initiation of the asthma phenotype.

Methods: We developed a color-coded real-time imaging model of cell migration into the lung using green fluorescent protein (GFP) and red fluorescent protein (RFP) transgenic CD4 T cells.

Results: Selective accumulation of antigen-specific CD4 T cells in the lungs was quantitatively imaged in a mouse model of asthma. The inhibition of accumulation by dexamethasone was imaged. Accumulating GFP^+ T_H2 cells formed foci in the lungs from 6 to 20 hours after antigen inhalation. This process was also inhibited by the administration of anti–intercellular adhesion molecule 1 or anti–vascular cell adhesion molecule 1 mAbs. Two days after inhalation of antigen, GFP^+ T_H2 cells were detected in the area of eosinophil infiltration.

Conclusion: Focus formation generated by accumulating antigen-specific T_H2 cells in the lung appeared to be a critical process in the initiation of the asthma phenotype. This new model enables the study of *in vivo* cell biology of airway inflammation and novel drug discovery for lung inflammatory diseases. (J Allergy Clin Immunol 2010;125:461-8.)

Key words: *Real-time in vivo cellular imaging, cellular dynamics, T_H2 cells, mouse model of asthma, focus formation, airway inflammation, GFP, ICAM-1, VCAM-1*

Abbreviations used
DEX: Dexamethasone
GFP: Green fluorescent protein
H&E: Hematoxylin and eosin
ICAM-1: Intercellular adhesion molecule 1
NIH: National Institutes of Health
RFP: Red fluorescent protein
TCR: T-cell receptor
Tg: Transgenic
VCAM-1: Vascular cell adhesion molecule 1

Lung inflammatory diseases such as asthma are major public health problems that have increased markedly in prevalence in the past 3 decades.[1] Asthma is characterized by a chronic inflammatory disease of the lower airways that causes airway hyperresponsiveness to a wide variety of specific and nonspecific stimuli.[2,3] The cardinal features of acute asthma are airway inflammation predominated by eosinophils, hypersecretion of mucus, and airway hyperresponsiveness. A critical role for $CD4^+$ T_H2 cells in the pathogenesis of acute asthma has been demonstrated in studies of human asthma as well as in animal models of allergic airway inflammation.[4-10] Previous investigations have studied T-cell migration during allergic reactions by using an adoptive cell transfer system.[11-13] The administration of anti–intercellular adhesion molecule 1 (ICAM-1) or anti–vascular cell adhesion molecule 1 (VCAM-1) antibody resulted in the inhibition of eosinophilic airway inflammation.[14] However, the *in vivo* dynamics of cell migration into the lung during inflammation in living animals is poorly understood because of the lack of an appropriate *in vivo* cellular imaging model. The use of fluorescent proteins for imaging, which we pioneered, allowed us to monitor cell migration *in vivo*.[15] Green fluorescent protein (GFP) and red fluorescent protein (RFP) were used to label living cells genetically *in vivo* as well as *in vitro*[16,17] and served as a powerful tool to monitor the migration of specific lymphocytes in live animals.

We report here a novel *in vivo* real-time color-coded cellular imaging model to visualize the dynamics of migration of T cells in a mouse model of asthma. We have found that accumulating T_H2 cells formed foci in the lungs 6 to 20 hours after allergen inhalation. Focus formation was dependent on ICAM-1 and VCAM-1 and appeared to determine the site of eosinophilic infiltration, indicating that T_H2-cell focus formation is a critical process during the initiation of airway inflammation in this animal model.

METHODS

Mice

C57BL/6 were purchased from Charles River Laboratories (Wilmington, MA). C57BL/6-transgenic (Tg) (CAG-EGFP)C14-Y01-FM131Osb (GFP Tg, C57BL/6 background) mice expressed an enhanced GFP in all tissue under the

From the Departments of [a]Immunology and [b]Molecular Genetics, Graduate School of Medicine, Chiba University; [c]the Department of Microbiology and Immunology, Yamaguchi University School of Medicine; [d]AntiCancer, Inc, San Diego; and [e]the Department of Surgery, University of California San Diego.

Supported in part by the Global Center of Excellence (COE) Program (Global Center for Education and Research in Immune System Regulation and Treatment), Monbukagakusho (MEXT), Japan, and grants from the Ministry of Education, Culture, Sports, Science and Technology (Japan).

Disclosure of potential conflict of interest: The authors have declared that they have no conflict of interest.

Received for publication April 15, 2009; revised July 26, 2009; accepted for publication August 2, 2009.

Available online December 25, 2009.

Reprint requests: Toshinori Nakayama, MD, PhD, Department of Immunology (H3), Graduate School of Medicine, Chiba University, 1-8-1 Inohana, Chuo-ku, Chiba, 260-8670 Japan. E-mail: tnakayama@faculty.chiba-u.jp.

0091-6749/$36.00

doi:10.1016/j.jaci.2009.09.016

control of the β-actin promoter.[16] C57BL/6 background RFP Tg mice expressed RFP (DsRed-2) under the control of the chicken β-actin promoter and cytomegalovirus enhancer.[17,18] Ovalbumin-specific T-cell receptor αβ transgenic (OT II Tg) mice[19] were maintained under specific pathogen-free conditions. All animal care was carried out in accordance with the National Institutes of Health (NIH) guidelines (NIH assurance no. A3873-01) at AntiCancer, Inc. and the guidelines of Chiba University. All animal experiments were performed at AntiCancer Inc.

In vitro T_H2-cell differentiation cultures

Green fluorescent protein Tg x OT II Tg $CD44^{low}$ CD4 T cells (2×10^5) were purified by cell sorting and stimulated with antigenic ovalbumin peptide (Loh 15, 1 μmol/L) and irradiated (30 Gy) syngeneic antigen-presenting cells (1×10^6) in the presence of exogenous IL-4 as described previously.[20]

Ovalbumin sensitization, cell transfer, and ovalbumin inhalation

The GFP or RFP Tg mice were immunized intraperitoneally with 250 μg ovalbumin (chicken egg albumin from Sigma St Louis, Mo) in 4 mg aluminum hydroxide gel (alum) on days 0 and 7. Splenic CD4 T cells from ovalbumin-sensitized GFP or RFP Tg mice were isolated by magnetic negative selection using a $CD4^+$ T-cell isolation kit (Miltenyi Biotec, Bergish Gladbach, Germany) on day 14, yielding a purity of >98%. These cells (2×10^7 cells) or ovalbumin-specific T_H2 cells (5×10^6 cells) were transferred intravenously through the tail vain to 8-week-old C57BL/6 recipient mice. One or 2 days later, the recipient mice inhaled aerosolized ovalbumin in saline (10 mg/mL) for 30 minutes with a supersonic nebulizer (NE-U07; Omron Co, Kyoto, Japan) as described previously.[21]

Fluorescence imaging of cell accumulation in the lung

The mice were killed by CO_2 asphyxiation at various times after ovalbumin inhalation. The lungs were removed, and GFP^+ cells that had accumulated in the excised lung were monitored by using an OV100 Small Animal Imaging System (Olympus Corp., Tokyo, Japan).[15,22,23]

Dexamethasone treatment

Splenic CD4 T cells (2×10^7 cells) were transferred intravenously through the tail vein to 8-week-old C57BL/6 recipient mice on day 14. One hour before the airway challenge by ovalbumin inhalation (on day 15), mice were injected intraperitoneally with dexamethasone (0.4, 1, or 4 mg/kg). The mice were exposed to allergen challenges on days 15, and transferred GFP^+ CD4 T cells were monitored on day 16. Where indicated, dexamethasone was injected 1 hour before (day 15) or 1 day after ovalbumin inhalation (day 16). Two days after OVA inhalation (day 17), GFP^+ CD4 T cells were monitored by using the OV100 Small Animal Imaging System.

Anti–ICAM-1 and anti–VCAM-1 antibody treatment

Ovalbumin-specific T_H2 cells (5×10^6 cells) were transferred intravenously through the tail vein of 8-week-old C57BL/6 recipient mice. Twenty-four hours before the airway challenge by ovalbumin inhalation, mice were injected intraperitoneally with 200 μg anti–ICAM-1 (YN1/1.7.4) or anti–VCAM-1 (429) mAbs.[14] One day after ovalbumin inhalation, transferred ovalbumin-specific T_H2 cells were monitored by using the OV100 Small Animal Imaging System.

In vivo imaging of lung infiltrating T cells by scanning laser microscopy

Control mice and mice given ovalbumin were prepared surgically at various indicated time points after ovalbumin administration for lung imaging. The mice were anesthetized and tracheostomized on the surgical bed and kept at 37°C. The right bronchus was clamped to stop movement during ventilation. The left lung was mechanically ventilated with O_2 at the normal respiratory rate to keep the mice alive. The clamped right lung was monitored with the IV100 scanning laser microscope (Olympus Corp., Tokyo, Japan). The IV100 microscope enabled imaging up to 100 μm depth from the surface of the lung. A 488-nm argon laser was used. To create an *in vivo* video image, images were recorded at 5-second intervals for 40 minutes. A focus was scored when more than 50% of the 2-dimentional area was occupied by the infiltrating GFP^+ cells. Crawling (motile) cells in the lung were defined as those that migrated or elongated to more than 50% of their diameter. The NIH Image software program (NIH Image J 1.41) was used for image analysis.

Lung histology and immunohistochemistry

The mice were killed by CO_2 asphyxiation at the indicated times after ovalbumin inhalation, and the lungs were infused with 10% (vol/vol) formalin in PBS or 4% (vol/vol) paraformaldehyde for fixation. The lung samples were sectioned, stained with hematoxylin and eosin (H&E), and examined for pathological changes under a light microscope at magnification ×50 or ×200.[7] Lung specimens were embedded in Tissue-Tek optimal cutting temperature compound (Sakura Fluelek, Tokyo, Japan), frozen in liquid nitrogen, and cut with a cryostat into 6-μm-thick sections. Endogenous peroxidase activity as well as nonspecific protein binding was sequentially blocked by using 0.6% hydrogen peroxide and Biotin-Blocking System reagent (DAKO, Glostrup, Denmark), respectively. The sections were incubated with hamster anti-GFP mAb (AdD Serotec, Oxford, UK) at 10 μg/mL overnight at 4°C and then were washed in TRIS-buffered saline with Tween. Bound antibody was detected by sequential incubation with biotinylated rabbit antihamster IgG and streptavidin–horseradish peroxidase followed by 3,3-diaminobenzidine (DAKOCytomation). The slides were then washed and counterstained with hematoxylin.

Statistical analysis

Experimental data were expressed as the means + SDs. The significance between 2 groups was determined by the 2-tailed Student *t* test.

RESULTS

Color-coded fluorescence imaging of selective accumulation of ovalbumin-primed CD4 T cells into the lung in an ovalbumin-induced acute-asthma mouse model

To examine the CD4 T-cell behavior in the lung of living mice in a mouse model of asthma, we developed a color-coded imaging model using GFP or RFP Tg CD4 T cells (Fig 1, *A*). Immediately after cell transfer, numerous transferred cells temporally and nonspecifically accumulated in the lung capillaries (data not shown). One day later, some of the cells remained in the lung with no significant difference between sensitized GFP^+ and non-sensitized RFP^+ cells (Fig 1, *B, left*; before inhalation). One day after ovalbumin inhalation, the number of GFP^+ CD4 T cells from ovalbumin-immunized mice increased significantly, and some of them formed foci (Fig 1, *B, center*; after inhalation). In contrast, the number of RFP^+ CD4 T cells from nonimmunized mice did not increase in the lung (Fig 1, *B and C*). These results indicate that CD4 T-cell migration into the lung after ovalbumin inhalation is ovalbumin priming–dependent. When we used the opposite color-coded immunization pattern, only the ovalbumin-primed RFP^+ CD4 T cells accumulated in the lung, not the nonprimed GFP^+ CD4 T cells (see this article's Fig E1, *A and B*, in the Online Repository at www.jacionline.org). These results indicate that the

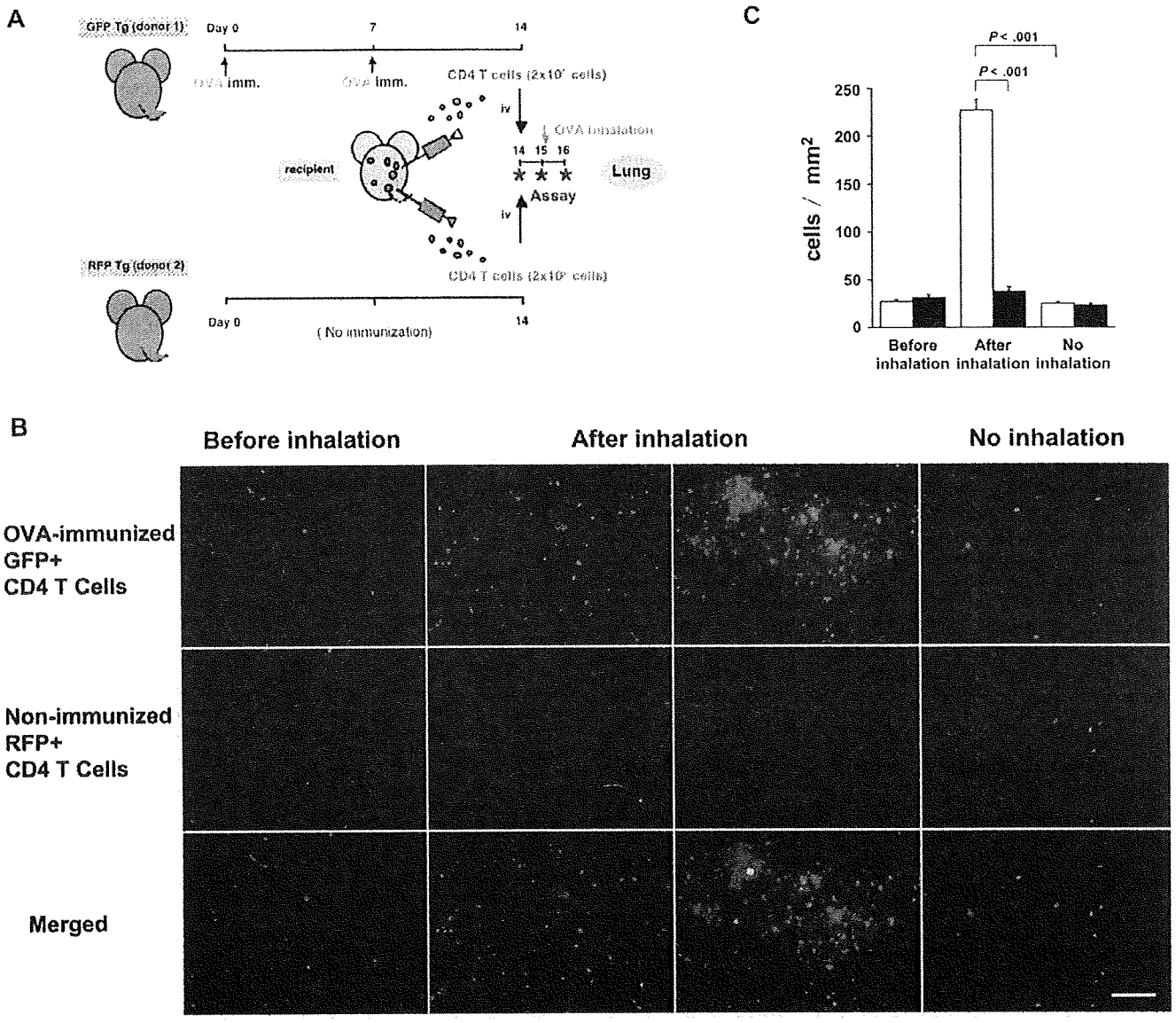

FIG 1. Color-coded fluorescence imaging of ovalbumin *(OVA)*-primed CD4 T-cell accumulation in the lung in the OVA-induced acute asthma model. **A,** A schematic overview of the study protocol for the induction of asthma. GFP Tg mice were sensitized with OVA on days 0 and 7. Splenic CD4 T cells from OVA-sensitized GFP Tg and nonsensitized RFP Tg mice were purified and injected into normal C57BL/6 mice on day 14. The recipient mice were exposed to airway challenge with aerosolized OVA on day 15. **B,** Color-coded images of GFP^+ and RFP^+ CD4 T cells. GFP^+ and RFP^+ CD4 T cells in the excised lung were monitored before OVA inhalation on day 15 and 24 hours after OVA inhalation on day 16 by using the OV100 Small Animal Mouse Imaging System. *Bar,* 100 μm. **C,** Summary of the accumulation of fluorescent cells. Data are from 15 fields from 3 mice with SD. *Open bar,* GFP; *closed bar,* RFP. $*P < .001$ by the Student's *t* test.

difference in accumulation is not fluorescent protein–dependent. Furthermore, we examined the migration of naive antigen-specific CD4 T cells in the lung. Ovalbumin-specific CD4 T cells were prepared from nonimmunized mice derived by crossing GFP Tg mice with OT II Tg mice, which have ovalbumin-specific, MHC class II–restricted αβ T-cell receptors.[19] Most of the CD4 T cells in the OT II Tg mice are ovalbumin-specific. Ovalbumin-specific CD4 T cells were transferred intravenously into normal C57BL/6 mice 24 hours before airway challenge with aerosolized ovalbumin. Twenty-four hrs after ovalbumin inhalation, GFP^+ cells in the excised lungs were monitored by fluorescence imaging. The number of GFP^+ OT II Tg–CD4 T cells did not increase in the lung (see this article's Fig E2 in the Online Repository at www.jacionline.org). These results indicate that even antigen-specific CD4 T cells do not accumulate in the lung after allergen challenge if the cells are not primed.

Imaging of ovalbumin-specific OT II–T_H2 cell accumulation into the lung and the generation of GFP^+ T_H2 cell foci in a mouse model of asthma

To investigate the dynamics of accumulating antigen-specific effector T cells in the lung of living mice in a mouse model of asthma, ovalbumin-specific T_H2 cells (OT II–Tg–T_H2) were

prepared *in vitro* from naive CD4 T cells obtained from GFP^+ OT II Tg mice. Ovalbumin-specific OT II–Tg–T_H2 cells expressing GFP were transferred intravenously into normal C57BL/6 mice. Immediately after cell transfer, numerous transferred cells temporally and nonspecifically accumulated in the lung capillaries (data not shown). Twenty-four hours after cell transfer, the recipient mice were exposed to allergen challenge with aerosolized ovalbumin. GFP^+ OT II–T_H2 cells were imaged under fluorescence microscopy at various time points as long as 24 hours after ovalbumin inhalation by excising the lung (Fig 2, *A*). The accumulation of GFP^+ OT II–T_H2 cells in the lung was detected beginning 6 hours after allergen inhalation. The maximum number of OT II–T_H2 cells accumulated between 18 and 24 hours. GFP^+ OT II–T_H2 cells formed small foci 6 hours after ovalbumin inhalation (Fig 2, *A*). The number of foci increased, and their mean size also increased at 12 hours. The number of foci in the lungs further increased (18 hours). Nonfocal GFP^+ cells also greatly increased in the lung. At 18 hours or later, the border of the foci became diffuse, and many foci appeared to be fused. For color-coded imaging of the migration of nonprimed CD4 T cells around the OT II–T_H2-cell foci, GFP^+ OT II–T_H2 cells and splenic CD4 T cells from nonsensitized RFP Tg mice were purified and intravenously transferred together into normal C57BL/6 mice 24 hours before airway challenge with aerosolized ovalbumin. Twenty-four hours after ovalbumin inhalation, GFP^+ and RFP^+ cells in the excised lungs were monitored by fluorescence imaging. The number of RFP^+ CD4 T cells from nonimmunized mice did not increase around the OT II–T_H2 cell foci (see this article's Fig E3 in the Online Repository at www.jacionline.org). These results indicate that unprimed CD4 T cells do not accumulate in the foci formed by antigen-specific T_H2 cells. We have performed time course experiments. Most antigen-specific T_H2 cells accumulated in the lung within 24 hours after antigen inhalation. The accumulated cells that formed foci remained as long as 72 hours after antigen inhalation (data not shown).

Real-time cellular dynamics of T_H2-cell accumulation in the lung of living mice in a mouse model of asthma

Real-time cellular dynamics of antigen-specific T_H2-cell accumulation into the lung was then imaged in living mice at the cellular level by using scanning laser fluorescence microscopy. To image this process, antigen-specific T_H2 cells generated *in vitro* from naive CD4 T cells of GFP^+ OT II Tg mice were transferred intravenously into normal C57BL/6 mice. The recipient mice were administered ovalbumin by inhalation. They were then anesthetized and tracheostomized, and the lung was exposed microsurgically at various time points after ovalbumin inhalation. First, to assess any changes in blood flow rates in the clamped right lung and ventilated left lung, fluorescent microspheres were infused before and after clamping and ventilation. The lungs were then monitored by fluorescence microscopy (see this article's Fig E4 in the Online Repository at www.jacionline.org). Thirty minutes after clamping and ventilation, blood flow rates in both lungs were comparable. The relative blood flow was still kept at more than 80% of that before clamping and ventilation. Thus, the relative blood flow rates in the clamped lung appeared not to be changed in this experimental system.

The clamped right lungs were then imaged with the IV100 scanning laser microscope. Before ovalbumin inhalation, no foci were observed in the lung (Fig 2, *B*; Table I; see this article's Video E1 in the Online Repository at www.jacionline.org). The rate of rolling GFP^+ T_H2 cells in the field was 14.7 + 1.5 cells/mm^2/30 min. Some of the rolling cells attached and accumulated in the field (7.0 + 1.5 cells/mm^2/30 min), and a similar amount of the T_H2 cells egressed from the field (7.0 + 1.0 cells/mm^2/30 min). These results suggest that the allergen-specific effector T cells were rolling in the lung vessels, and some were migrating into and accumulating in the lung, whereas some were migrating out of the lung. At time 0, the ratio of cells that accumulated and egressed from the field was equivalent, and the total cell number in the lung appeared to be maintained at a constant level. Only 10% of the T_H2 cells in the lung were crawling in this stable state (see this article's Video E2 in the Online Repository at www.jacionline.org). Six hours after ovalbumin inhalation, small foci were observed (Fig 2, *B, red asterisks*). By 6 hours, the number of rolling T_H2 cells greatly increased compared with the stable state (33.3 + 3.1 vs 14.7+1.5 cells/mm^2/30 min; Table I). GFP^+ T_H2-cell accumulation in the lung also increased (15.3 + 1.5 cells/mm^2/30 min; Table I; see this article's Video E3 in the Online Repository at www.jacionline.org). The degree of GFP^+ T_H2-cell egress from the field was similar to that observed in the stable state. By 6 hours, the ratio of crawling cells was observed to increase (30.5% from 10.0%). These observations suggest that the allergen-induced migration and accumulation of T_H2 cells into the lung began to be upregulated by 6 hours after ovalbumin inhalation. The formation of foci was also observed approximately 6 hours after ovalbumin inhalation. Twelve hours after ovalbumin inhalation, the foci became larger, and the number of T_H2 cells rolling in the field further increased (44.7 + 4.5 cells/mm^2/30 min; Table I; see this article's Video E4 in the Online Repository at www.jacionline.org). T_H2-cell accumulation in the lung also further increased (24.3 + 2.5 cells/mm^2/30 min). However, the degree of T_H2-cell egress from the field did not obviously change compared with that observed in the stable state (8.3 + 1.6 vs 7.0 + 1.0). At 12 hours after ovalbumin inhalation, 90% of the T_H2 cells accumulating in the field were crawling (see this article's Video E5 in the Online Repository at www.jacionline.org). Thus, allergen-induced migration and accumulation of T_H2 cells into the lung appeared to be highly upregulated at approximately 12 hours after ovalbumin inhalation. At 21 hours after ovalbumin inhalation, nonfocal T_H2 cells greatly increased (868.7 + 296.5 cells/mm^2/30 min at 21 hours). More than 95% of the accumulating cells were crawling at this time point. However, at 21 hours, T_H2 cells rolling into the field were apparently reduced (2.7 + 0.6 cells/mm^2/30 min; Table I; see this article's Video E6 in the Online Repository at www.jacionline.org). Therefore, the allergen-induced migration and accumulation of T_H2 cells into the lung reached maximum levels by 21 hours after ovalbumin inhalation. Between 6 and 12 hours after ovalbumin inhalation, the migrating T_H2 cells predominantly formed foci. Later, at 12 to 21 hours after ovalbumin inhalation, the T_H2 cells were observed to accumulate throughout the lung rather than form foci.

Effect of dexamethasone on the accumulation of ovalbumin-primed CD4 T cells in the lung in a mouse model of asthma

The color-coded imaging system was then used to determine the effect of dexamethasone, a potent drug that attenuates

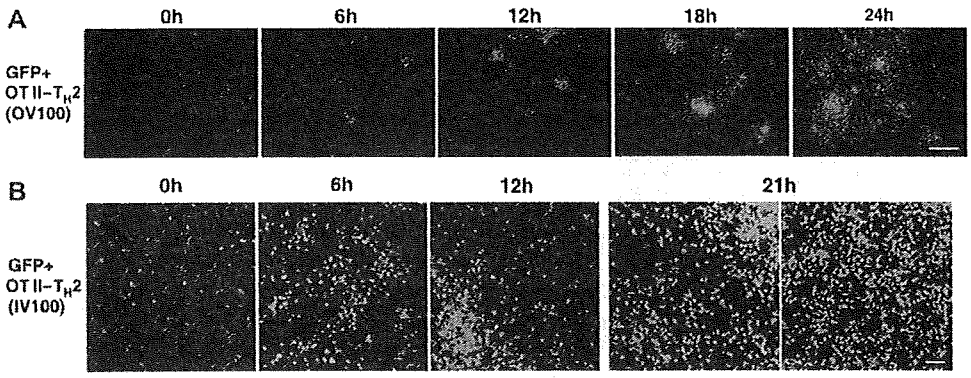

FIG 2. Imaging of ovalbumin-specific OT II-T_H2-cell accumulation in the lung and the generation of GFP^+ T_H2-cell foci after ovalbumin inhalation. GFP^+ OT II-T_H2 cells, differentiated *in vitro* from naive CD4 T cells from GFP^+ OT II Tg mice, were intravenously transferred into C57BL/6 mice. Two days later, the recipient mice were administered ovalbumin by inhalation. The mice were subjected to imaging at indicated time points after ovalbumin inhalation. GFP^+ T_H2 cells were imaged by using the OV100 Small Animal Imaging System **(A)** or the IV100 scanning laser imaging system **(B)**. *Red asterisks* indicate the site of focus formation. *Bar*, 300 μm *(A)* and 100 μm *(B)*. The results are representative of 5 *(A)* and 3 *(B)* experiments.

TABLE I. Summary of nonfocal OT II-T_H2 cell accumulation in the lung after ovalbumin inhalation

After ovalbumin inhalation	0 h	6 h	12 h	21 h
Cell number in nonfocal area (cells/mm^2)	57.7 ± 4.5	134.3 ± 16.9	226.0 ± 25.1	868.7 ± 296.5
Cells rolling in the blood vessel (cells/mm^2/30 min)	14.7 ± 1.5	33.3 ± 3.1	44.7 ± 4.5	2.7 ± 0.6
Cells accumulated in the field (cells/mm^2/30 min)	7.0 ± 1.5	15.3 ± 1.5	24.3 ± 2.5	1.3 ± 0.6
Cells egressed from the field (cells/mm^2/30 min)	7.0 ± 1.0	8.0 ± 1.5	8.3 ± 1.6	0.7 ± 0.6
Cells crawling in the field (%)	10.0	30.5	90.0	96.0

The data are presented as the mean cell number + SD from 3 independent experiments unless otherwise indicated.

allergic reactions, on the accumulation of allergen-primed CD4 T cells in the lung. Dexamethasone (0.4, 1, or 4 mg/kg) was administered intraperitoneally 1 hour before ovalbumin inhalation. GFP^+ CD4 T cells were monitored by fluorescence imaging 24 hours after ovalbumin inhalation. A marked dexamethasone dose-dependent decrease in the number of infiltrated CD4 T cells was observed in the excised lung (Fig 3, *A and B*). These results suggest that the efficacy of dexamethasone in inhibiting the development of ovalbumin-induced airway inflammation was, at least in part, a result of the inhibition of CD4 T-cell accumulation into the lung. Dexamethasone was then administered intraperitoneally after ovalbumin inhalation (on day 16), and GFP^+ CD4 T cells were monitored by fluorescence imaging 1 day later. The extent of infiltration of GFP^+ CD4 T cells was again observed to decrease significantly (Fig 3, *C and D*). These results indicate that the infiltration of CD4 T cells was reduced if dexamethasone was administered even after the onset of airway inflammation.

Contribution of adhesion molecules to the generation of T_H2-cell foci in the lung in a mouse model of asthma

We next assessed the contribution of adhesion molecules to the generation of T_H2-cell foci in the lung in a mouse model of asthma. The blockage of ICAM-1 and VCAM-1 by antibodies to these molecules is known to inhibit airway inflammation.[14] To test the role of ICAM-1 and VCAM-1 in our model, GFP^+ OT II-T_H2 cells were transferred intravenously into normal C57BL/6 mice. One day before ovalbumin inhalation, mice were injected intraperitoneally with 200 μg anti–ICAM-1 (YN1/1.7.4) or anti–VCAM-1 (429) mAbs. One day after ovalbumin inhalation, transferred ovalbumin-specific GFP^+ T_H2 cells were monitored by using fluorescence imaging. The generation of GFP^+ T_H2-cell foci in the lung was substantially inhibited by treatment with anti–ICAM-1 and anti–VCAM-1 mAbs (Fig 3, *E and F*). Our model demonstrates that ICAM-1 and VCAM-1 play an essential role in focus formation by the control of T_H2-cell migration in the lung. Thus, T_H2 focus formation appears to be critical in the development of allergic airway inflammation in this animal model.

Eosinophilic infiltration and GFP^+ T_H2-cell infiltration into the lung in a mouse model of asthma

Previous studies in animal models suggest a T_H2 paradigm for allergic diseases, with an increased activation of T_H2 cells that produce T_H2 cytokines, thereby resulting in the recruitment and activation of eosinophils. Marked eosinophilic infiltration is characteristic 2 or 3 days after allergen challenge in animal models of allergic airway inflammation.[7,9,10] The foci formed by T_H2 cells observed in the current study and accumulation of eosinophils may be coincidental because our results showed

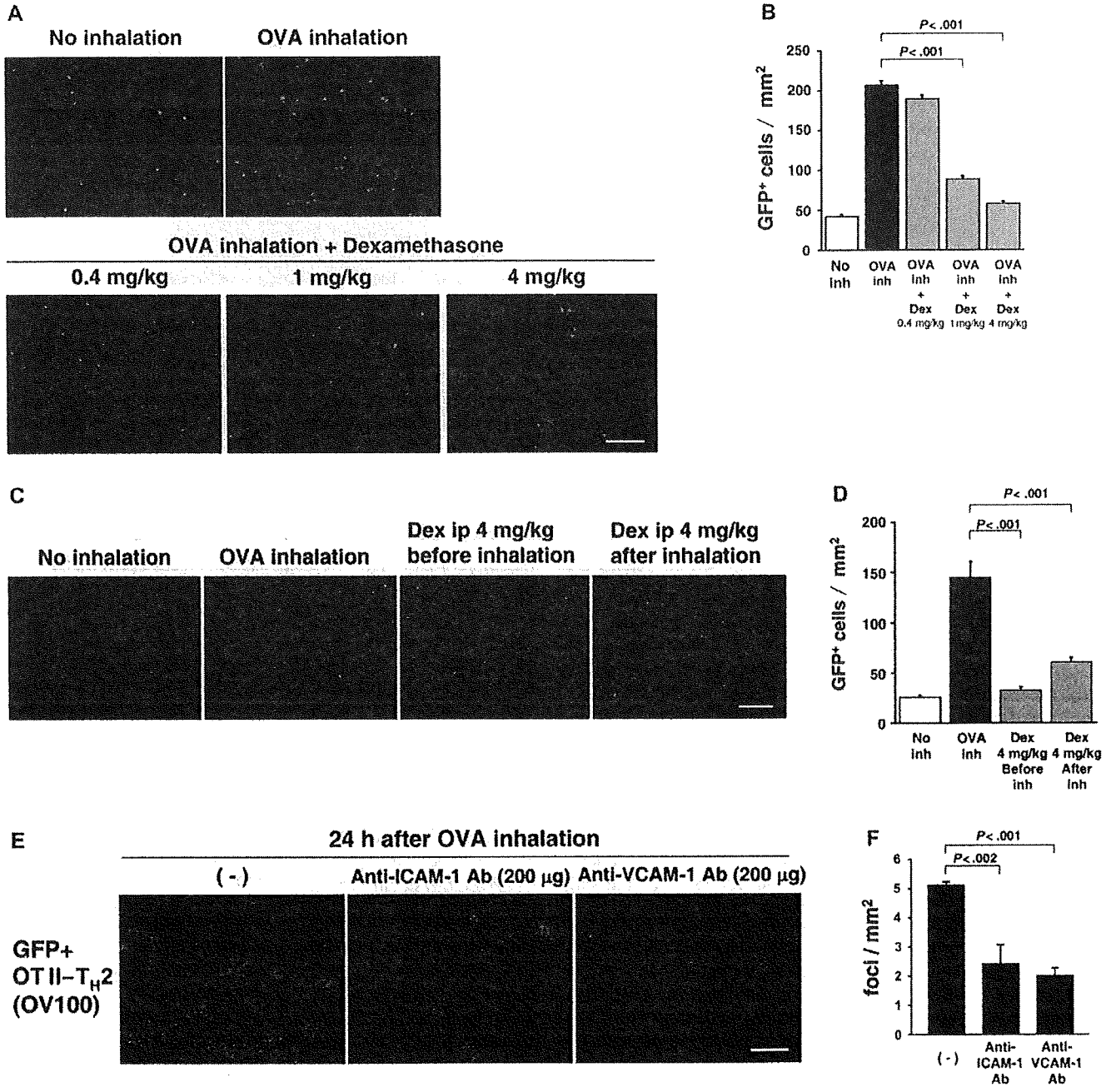

FIG 3. Effects of dexamethasone, anti–ICAM-1, and anti–VCAM-1 treatment on CD4 T-cell accumulation in the lung after ovalbumin (OVA) inhalation. **A,** Allergic airway inflammation was induced as in Fig 1, *A*. Three different doses of dexamethasone (DEX) were injected intraperitoneally 1 hour before OVA inhalation. Twenty-four hours after inhalation (day 16), GFP^+ CD4 T cells were monitored by using the OV100 Small Animal Imaging System. *Bar,* 100 μm. **B,** Summary of the accumulation of fluorescent cells of *A*. Data are from 15 fields from 3 mice with SD. $P < .001$ by the Student's *t* test. **C,** Dexamethasone was injected intraperitoneally 1 hour before or 1 day after OVA inhalation. Two days after inhalation, GFP^+ CD4 T cells were monitored in the excised lung by using the OV100 Small Animal Imaging System. *Bar,* 100 μm. **D,** Summary of the accumulation of fluorescent cells of *C*. The data are from 15 fields from 3 mice with SD. $P < .001$ by the Student's *t* test. **E,** Allergic airway inflammation was induced as in Fig 2, *A*. Anti–ICAM-1 or anti–VCAM-1 mAb was injected intraperitoneally 24 hours before OVA inhalation. Twenty-four hours after OVA inhalation, GFP^+ OT II–T_H2 cells were monitored. *Bar,* 100 μm. **F,** Summary of the generation of T_H2-cell foci in *E*. Data are from 12 fields from 3 mice with SD. $P < .002$, $P < .001$ by the Student's *t* test.

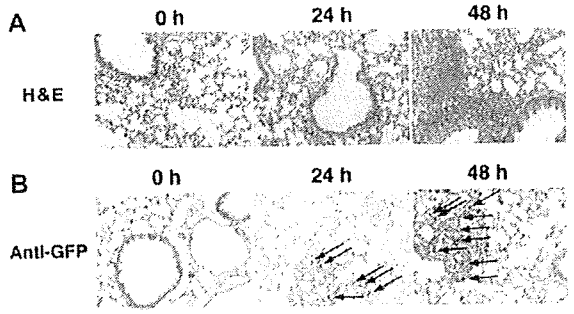

FIG 4. Eosinophilic infiltration and GFP^+ T_H2-cell infiltration into the lung in a mouse model of asthma. **A,** The lung specimens were fixed at indicated time point after ovalbumin inhalation and stained with H&E. A representative H&E staining pattern in each group is shown. Magnification ×200. **B,** Representative immunohistochemical staining for GFP is shown. Magnification ×200. *Arrows* indicate some of the representative GFP-positive cells. The results are representative of 3 experiments.

that antigen-specific T_H2 cells accumulated and formed foci in the lung after allergen inhalation. GFP^+ OT I–T_H2 cells were intravenously transferred into C57BL/6 mice, and 2 days later, the recipient mice were exposed to ovalbumin. Typical peribronchiolar and perivascular infiltration and focus formation by eosinophils were observed 48 hours after ovalbumin inhalation (Fig 4, *A*). The infiltrated OT II–T_H2 cells were monitored by immunohistochemistry analysis with an anti-GFP antibody. We observed GFP^+ transferred T_H2 cells in the region of subsequent eosinophilic infiltration (Fig 4, *B*). These results, in conjunction with the results of our time course experiments (Fig 2), indicate that antigen-specific T_H2 cells accumulate and form foci in the lung before the marked infiltration of eosinophils and thus regulate the initiation of inflammatory processes in this animal model.

DISCUSSION

The behavior of T cells during airway inflammation in mouse models of asthma has been investigated by using flow cytometry and immunohistochemistry.[24-28] These studies showed that T cells migrate into the lung after allergen challenge, but the studies did not address how and when they migrate into the lung or whether only antigen-specific effector T cells migrate into the lung. Several investigators performed lung imaging in a serial but static manner. Hutchison et al[29] have used serial tissue sectioning to describe the time course of proliferating CD4 T cells in the lung and its draining lymph nodes. Bhattacharya's group[30,31,32] imaged whole excised lungs to study signaling by lung resident cells. Until now, the *in vivo* dynamics of cell invasion of the lung during inflammation in living animals has been poorly understood because it has been difficult to arrest motion in the lung as a result of the beating heart or movement during respiration. Our novel imaging model has overcome these problems and has demonstrated, for the first time, the dynamics of migration of allergen-specific T_H2 cells into the lung after allergen inhalation in living animals at the cellular level using the adoptive transfer of GFP^+ T cells.

With this novel imaging model, several important findings are demonstrated. We have shown for the first time T_H2-cell focus formation in the lung, a cellular immunologic event occurring during the initiation of airway inflammation (Fig 2). In addition, we demonstrate that unprimed CD4 T cells and naive antigen-specific CD4 T cells did not accumulate around the foci (Fig 1; Figs E1-E3), indicating that the molecules specifically expressed on activated effector T_H2 cells play an important role in migration and focus formation. Moreover, T_H2-cell focus formation occurred before eosinophilic infiltration and thus may determine the eosinophilic inflammatory site (Figs 2 and 4). Focus formation was inhibited by the administration of anti–ICAM-1 and anti–VCAM-1 antibodies (Fig 3, *E and F*), both of which are able to block the induction of eosinophilic airway inflammation, indicating that focus formation is a critical process during the induction of the asthma phenotype.

Several groups have shown time-lapse microscopy of GFP-labeled and/or RFP-labeled cancer cells in live mice. Hoffman's group[22,23] has demonstrated *in vivo* imaging of intracapillary and intralymphatic cancer cell trafficking behavior. Condeelis' group[33] has used *in vivo* imaging to determine molecular mechanisms of cancer metastasis.

Many groups have reported *in vivo* imaging of lymphoid tissues such as lymph nodes, spleen, and bone marrow to visualize antigen presentation and T-cell migration.[34-41] To visualize the cells *in vivo*, they must be labeled by appropriate dyes or express fluorescent proteins. In most of the reports of *in vivo* imaging of lymphoid tissues, T cells were labeled by using appropriate dyes and transferred into recipient mice, although a possible difference in the migration behavior of the cells that were labeled by dyes has been suggested.[42] In our study, we prepared ovalbumin-specific T_H2 cells expressing GFP from GFP Tg mice[16] and transferred the cells intravenously into normal recipient mice. Another technical issue could be the difference in the migration between antigen-specific cells that were injected into the mice before imaging and antigen-specific T cells that were resident in the imaged mice. In the near future, the behavior of antigen-specific T_H2 cells that were resident in the imaged mice will be investigated.

This model allows investigators to monitor the migration of inflammatory lymphocytes into the lung in a real-time manner in live animals and thus provides a new strategy to study the *in vivo* cell biology of inflammatory lung diseases such as asthma. This method can be also applied to various bacteria-induced and virus-induced inflammatory lung diseases, including tuberculosis and influenza virus–induced pneumonia, and to screen for more effective drugs for these respiratory diseases.

We are grateful to Drs Tatsuo kinashi, Takashi Saito, Larry Samelson, and Ronald Germain for the valuable suggestions during manuscript preparation. We also thank Mr Jose Reynoso for help with the animal studies.

Key messages

- We established a novel *in vivo* real-time color-coded cellular imaging model to visualize the dynamics of migration of T cells in the lung in a mouse model of asthma.
- Accumulating T_H2 cells formed foci in the lungs 6 to 20 hours after allergen inhalation.
- The focus formation was dependent on ICAM-1 and VCAM-1 and appeared to determine the site of eosinophilic infiltration.
- T_H2-cell focus formation appears to be a critical process in the induction of allergic airway inflammation in this animal model.

REFERENCES

1. Eder W, Ege MJ, von Mutius E. The asthma epidemic. N Engl J Med 2006;355: 2226-35.
2. McFadden ER Jr, Gilbert IA. Asthma. N Engl J Med 1992;327:1928-37.
3. Busse WW, Lemanske RF Jr. Asthma. N Engl J Med 2001;344:350-62.
4. Hamelmann E, Gelfand EW. IL-5-induced airway eosinophilia—the key to asthma? Immunol Rev 2001;179:182-91.
5. Lloyd CM, Gonzalo JA, Coyle AJ, Gutierrez-Ramos JC. Mouse models of allergic airway disease. Adv Immunol 2001;77:263-95.
6. Elias JA, Lee CG, Zheng T, Ma B, Homer RJ, Zhu Z. New insights into the pathogenesis of asthma. J Clin Invest 2003;111:291-7.
7. Kamata T, Yamashita M, Kimura M, Murata K, Inami M, Shimizu C, et al. src homology 2 domain-containing tyrosine phosphatase SHP-1 controls the development of allergic airway inflammation. J Clin Invest 2003;111:109-19.
8. Wills-Karp M. Interleukin-13 in asthma pathogenesis. Immunol Rev 2004;202: 175-90.
9. Cohn L, Elias JA, Chupp GL. Asthma: mechanisms of disease persistence and progression. Annu Rev Immunol 2004;22:789-815.
10. Umetsu DT, DeKruyff RH. The regulation of allergy and asthma. Immunol Rev 2006;212:238-55.
11. Cohn L, Homer RJ, Marinov A, Rankin J, Bottomly K. Induction of airway mucus production By T helper 2 (Th2) cells: a critical role for interleukin 4 in cell recruitment but not mucus production. J Exp Med 1997;186:1737-47.
12. Hansen G, Berry G, DeKruyff RH, Umetsu DT. Allergen-specific Th1 cells fail to counterbalance Th2 cell-induced airway hyperreactivity but cause severe airway inflammation. J Clin Invest 1999;103:175-83.
13. Kaminuma O, Fujimura H, Fushimi K, Nakata A, Sakai A, Chishima S, et al. Dynamics of antigen-specific helper T cells at the initiation of airway eosinophilic inflammation. Eur J Immunol 2001;31:2669-79.
14. Nakajima H, Sano H, Nishimura T, Yoshida S, Iwamoto I. Role of vascular cell adhesion molecule 1/very late activation antigen 4 and intercellular adhesion molecule 1/lymphocyte function-associated antigen 1 interactions in antigen-induced eosinophil and T cell recruitment into the tissue. J Exp Med 1994;179:1145-54.
15. Hoffman RM. The multiple uses of fluorescent proteins to visualize cancer in vivo. Nat Rev Cancer 2005;5:796-806.
16. Okabe M, Ikawa M, Kominami K, Nakanishi T, Nishimune Y. Green mice' as a source of ubiquitous green cells. FEBS Lett 1997;407:313-9.
17. Vintersten K, Monetti C, Gertsenstein M, Zhang P, Laszlo L, Biechele S, et al. Mouse in red: red fluorescent protein expression in mouse ES cells, embryos, and adult animals. Genesis 2004;40:241-6.
18. Yang M, Reynoso J, Bouvet M, Hoffman RM. A transgenic red fluorescent protein-expressing nude mouse for color-coded imaging of the tumor microenvironment. J Cell Biochem 2009;106:279-84.
19. Barnden MJ, Allison J, Heath WR, Carbone FR. Defective TCR expression in transgenic mice constructed using cDNA-based alpha- and beta-chain genes under the control of heterologous regulatory elements. Immunol Cell Biol 1998;76:34-40.
20. Hasegawa A, Miki T, Hosokawa H, Hossain MB, Shimizu C, Hashimoto K, et al. Impaired GATA3-dependent chromatin remodeling and Th2 cell differentiation leading to attenuated allergic airway inflammation in aging mice. J Immunol 2006;176:2546-54.
21. Hirahara K, Yamashita M, Iwamura C, Shinoda K, Hasegawa A, Yoshizawa H, et al. Repressor of GATA regulates TH2-driven allergic airway inflammation and airway hyperresponsiveness. J Allergy Clin Immunol 2008;122:512-20.
22. Yamauchi K, Yang M, Jiang P, Xu M, Yamamoto N, Tsuchiya H, et al. Development of real-time subcellular dynamic multicolor imaging of cancer-cell trafficking in live mice with a variable-magnification whole-mouse imaging system. Cancer Res 2006;66:4208-14.
23. Hayashi K, Jiang P, Yamauchi K, Yamamoto N, Tsuchiya H, Tomita K, Moossa AR, Bouvet M, Hoffman RM. Real-time imaging of tumor-cell shedding and trafficking in lymphatic channels. Cancer Res 2007;67:8223-8.
24. Catron DM, Rusch LK, Hataye J, Itano AA, Jenkins MK. CD4 + T cells that enter the draining lymph nodes after antigen injection participate in the primary response and become central-memory cells. J Exp Med 2006;203:1045-54.
25. Kohlmeier JE, Woodland DL. Memory T cell recruitment to the lung airways. Curr Opin Immunol 2006;18:357-62.
26. Mathew A, Medoff BD, Carafone AD, Luster AD. Cutting edge: Th2 cell trafficking into the allergic lung is dependent on chemoattractant receptor signaling. J Immunol 2002;169:651-5.
27. Wells JW, Cowled CJ, Giorgini A, Kemeny DM, Noble A. Regulation of allergic airway inflammation by class I-restricted allergen presentation and CD8 T-cell infiltration. J Allergy Clin Immunol 2007;119:226-34.
28. Xu B, Wagner N, Pham LN, Magno V, Shan Z, Butcher EC, et al. Lymphocyte homing to bronchus-associated lymphoid tissue (BALT) is mediated by L-selectin/PNAd, alpha4beta1 integrin/VCAM-1, and LFA-1 adhesion pathways. J Exp Med 2003;197:1255-67.
29. Hutchison S, Choo-Kang BS, Gibson VB, Bundick RV, Leishman AJ, Brewer JM, et al. An investigation of the impact of the location and timing of antigen-specific T cell division on airways inflammation. Clin Exp Immunol 2009;155:107-16.
30. Ichimura H, Parthasarathi K, Lindert J, Bhattacharya J. Lung surfactant secretion by interalveolar Ca2+ signaling. Am J Physiol Lung Cell Mol Physiol 2006; 291:L596-601.
31. Kuebler WM, Parthasarathi K, Lindert J, Bhattacharya J. Real-time lung microscopy. J Appl Physiol 2007;102:1255-64.
32. Hayashi K, Jiang P, Yamauchi K, Yamamoto N, Tsuchiya H, Tomita K, et al. Real-time imaging of tumor-cell shedding and trafficking in lymphatic channels. Cancer Res 2007;67:8223-8.
33. Wang W, Wyckoff JB, Goswami S, Wang Y, Sidani M, Segall JE, et al. Coordinated regulation of pathways for enhanced cell motility and chemotaxis is conserved in rat and mouse mammary tumors. Cancer Res 2007;67:3505-11.
34. Miller MJ, Safrina O, Parker I, Cahalan MD. Imaging the single cell dynamics of CD4 + T cell activation by dendritic cells in lymph nodes. J Exp Med 2004;200:847-56.
35. Miller MJ, Wei SH, Parker I, Cahalan MD. Two-photon imaging of lymphocyte motility and antigen response in intact lymph node. Science 2002;296:1869-73.
36. Bajenoff M, Egen JG, Koo LY, Laugier JP, Brau F, Glaichenhaus N, et al. Stromal cell networks regulate lymphocyte entry, migration, and territoriality in lymph nodes. Immunity 2006;25:989-1001.
37. Bousso P, Robey E. Dynamics of CD8 + T cell priming by dendritic cells in intact lymph nodes. Nat Immunol 2003;4:579-85.
38. Mempel TR, Henrickson SE, Von Andrian UH. T-cell priming by dendritic cells in lymph nodes occurs in three distinct phases. Nature 2004;427:154-9.
39. Hugues S, Scholer A, Boissonnas A, Nussbaum A, Combadiere C, Amigorena S, et al. Dynamic imaging of chemokine-dependent CD8 + T cell help for CD8 + T cell responses. Nat Immunol 2007;8:921-30.
40. Schwickert TA, Lindquist RL, Shakhar G, Livshits G, Skokos D, Kosco-Vilbois MH, et al. In vivo imaging of germinal centres reveals a dynamic open structure. Nature 2007;446:83-7.
41. Cavanagh LL, Bonasio R, Mazo IB, Halin C, Cheng G, van der Velden AW, et al. Activation of bone marrow-resident memory T cells by circulating, antigen-bearing dendritic cells. Nat Immunol 2005;6:1029-37.
42. Germain RN, Miller MJ, Dustin ML, Nussenzweig MC. Dynamic imaging of the immune system: progress, pitfalls and promise. Nat Rev Immunol 2006;6:497-507.